Since January 2020 Elsevier has created a COVID-19 resource centre with free information in English and Mandarin on the novel coronavirus COVID-19. The COVID-19 resource centre is hosted on Elsevier Connect, the company's public news and information website.

Article

Immunity

Analysis of a Therapeutic Antibody Cocktail Reveals Determinants for Cooperative and Broad Ebolavirus Neutralization

Graphical Abstract

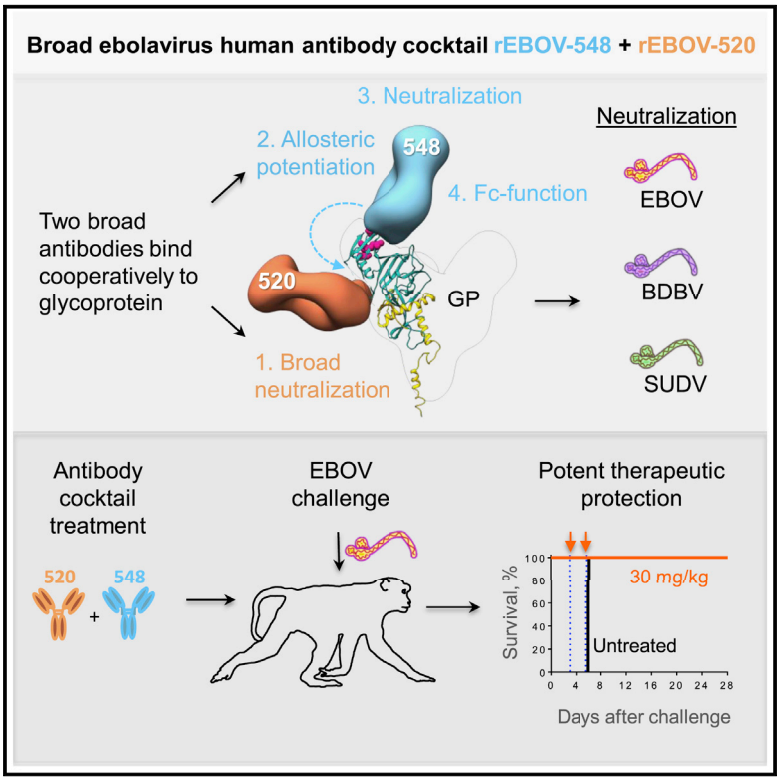

Highlights

- Human mAbs of two epitope specificities bind cooperatively to the ebolavirus GP
- Cooperativity is mediated by a mAb that enhances binding to a vulnerable GP epitope
- A two-mAb cocktail exhibits enhanced potency against heterologous ebolaviruses
- Two 30 mg/kg doses of the cocktail fully protected non-human primates (NHPs) challenged with EBOV

Authors

Pavlo Gilchuk, Charles D. Murin, Jacob C. Milligan, ..., Thomas W. Geisbert, Andrew B. Ward, James E. Crowe, Jr.

Correspondence

james.crowe@vumc.org

In Brief

Cooperative interactions of monoclonal antibodies (mAbs) with viral antigens are poorly understood. Gilchuk et al. perform structural and functional analysis of cooperativity in a cocktail of two human mAbs, recognizing major epitopes of ebolavirus glycoprotein (GP), and define cooperative binding of the GP as a mechanism for enhanced ebolavirus neutralization.

Gilchuk et al., 2020, Immunity *52*, 388–403
February 18, 2020
https://doi.org/10.1016/j.immuni.2020.01.001

CellPress

CellPress

Immunity
Article

Analysis of a Therapeutic Antibody Cocktail Reveals Determinants for Cooperative and Broad Ebolavirus Neutralization

Pavlo Gilchuk,[1,16] Charles D. Murin,[2,16] Jacob C. Milligan,[3] Robert W. Cross,[4,5] Chad E. Mire,[4,5] Philipp A. Ilinykh,[4,6] Kai Huang,[4,6] Natalia Kuzmina,[4,6] Pilar X. Altman,[3] Sean Hui,[3] Bronwyn M. Gunn,[7] Aubrey L. Bryan,[8] Edgar Davidson,[8] Benjamin J. Doranz,[8] Hannah L. Turner,[2] Tanwee Alkutkar,[2] Robin Flinko,[9] Chiara Orlandi,[9] Robert Carnahan,[1] Rachel Nargi,[1] Robin G. Bombardi,[1] Megan E. Vodzak,[1] Sheng Li,[10] Adaora Okoli,[11] Morris Ibeawuchi,[11] Benjamin Ohiaeri,[11] George K. Lewis,[9] Galit Alter,[7] Alexander Bukreyev,[4,5,6] Erica Ollmann Saphire,[3,12] Thomas W. Geisbert,[4,5] Andrew B. Ward,[2] and James E. Crowe, Jr.[1,13,14,15,*]

[1]Vanderbilt Vaccine Center, Vanderbilt University Medical Center, Nashville, TN 37232, USA
[2]Department of Integrative Structural and Computational Biology, The Scripps Research Institute, La Jolla, CA 92037, USA
[3]Department of Immunology and Microbiology, The Scripps Research Institute, La Jolla, CA 92037, USA
[4]Galveston National Laboratory, Galveston, TX 77550, USA
[5]Department of Microbiology & Immunology, University of Texas Medical Branch, Galveston, TX 77555, USA
[6]Department of Pathology, University of Texas Medical Branch, Galveston, TX 77555, USA
[7]Ragon Institute of MGH, MIT, and Harvard, Cambridge, MA 02139, USA
[8]Integral Molecular, Inc., Philadelphia, PA 19104, USA
[9]Division of Vaccine Research, Institute of Human Virology, University of Maryland School of Medicine, Baltimore, MD 21201, USA
[10]Department of Medicine, University of California, San Diego, San Diego, CA 92093, USA
[11]First Consultants Medical Center, Lagos, Nigeria
[12]The Skaggs Institute for Chemical Biology, The Scripps Research Institute, La Jolla, CA 92037, USA
[13]Department of Pathology, Microbiology, and Immunology, Vanderbilt University Medical Center, Nashville, TN 37232, USA
[14]Department of Pediatrics, Vanderbilt University Medical Center, Nashville, TN 37232, USA
[15]Lead Contact
[16]These authors contributed equally
*Correspondence: james.crowe@vumc.org
https://doi.org/10.1016/j.immuni.2020.01.001

SUMMARY

Structural principles underlying the composition of protective antiviral monoclonal antibody (mAb) cocktails are poorly defined. Here, we exploited antibody cooperativity to develop a therapeutic mAb cocktail against Ebola virus. We systematically analyzed the antibody repertoire in human survivors and identified a pair of potently neutralizing mAbs that cooperatively bound to the ebolavirus glycoprotein (GP). High-resolution structures revealed that in a two-antibody cocktail, molecular mimicry was a major feature of mAb-GP interactions. Broadly neutralizing mAb rEBOV-520 targeted a conserved epitope on the GP base region. mAb rEBOV-548 bound to a glycan cap epitope, possessed neutralizing and Fc-mediated effector function activities, and potentiated neutralization by rEBOV-520. Remodeling of the glycan cap structures by the cocktail enabled enhanced GP binding and virus neutralization. The cocktail demonstrated resistance to virus escape and protected non-human primates (NHPs) against Ebola virus disease. These data illuminate structural principles of antibody cooperativity with implications for development of antiviral immunotherapeutics.

INTRODUCTION

Human monoclonal antibodies (mAbs) are promising therapeutic molecules that can be used for the prevention or treatment of viral infectious diseases. In recent years, advances in human B cell isolation techniques have led to the identification of large numbers of therapeutic mAb candidates against many life-threatening viral pathogens. These targets include antigenically variable viruses, such as human immunodeficiency virus (HIV) (Sok and Burton, 2018) and influenza virus (Laursen and Wilson, 2013), or newly emerging pathogens with high epidemic potential, including Ebola virus (Bornholdt et al., 2016), Marburg virus (Flyak et al., 2015), Zika virus (Sapparapu et al., 2016; Stettler et al., 2016; Wang et al., 2016b), Lassa virus (Robinson et al., 2016), Middle East respiratory syndrome coronavirus (MERS-CoV) (Corti et al., 2016b), poxviruses (Gilchuk et al., 2016), Nipah virus (Geisbert et al., 2014), and many other medically important viruses. Over 25 antiviral human mAbs are now being evaluated as human therapeutics in clinical trials (Walker and Burton, 2018), including several for ebolavirus therapy (NIH, 2019).

Antibodies can mediate protection by direct virus neutralization and/or by engagement of innate immune cells via their Fc receptors (FcRs) (Crowe, 2017; Lu et al., 2018). Potent neutralization, broad reactivity, and protective capacity are desirable mAb features, which could be used to select leads for development as a monotherapy or cocktail. A cocktail

might offer greater efficacy and resistance to viral escape (Corti et al., 2016; Keeffe et al., 2018; Wec et al., 2019), but the molecular and structural basis for the optimal combination of mAbs is ill-defined. Current mAb discovery approaches typically are focused on antibody variable fragment (Fv)-region-mediated biological functions of single isolated mAbs (e.g., binding and neutralization) or Fc-region-mediated effector functions (Walker and Burton, 2018). Molecular interactions in which two or more mAbs recognize the same antigen in an enhanced (e.g., cooperative or synergistic) fashion are less well investigated, but these interactions might contribute greatly to the overall efficacy of protective cocktails (Carlsen et al., 2014; Doria-Rose et al., 2012; Howell et al., 2017; Mascola et al., 1997). One key challenge that impedes progress in this area is that the structural determinants of cooperativity by neutralizing antibodies are poorly understood. Development of synergistic mAb cocktails against viruses with high antigenic variability, including HIV, hepatitis C, norovirus, influenza virus, or Ebola virus, is also thwarted by the fact that only a small subset of virus-specific mAbs available for incorporation in cocktails is broadly cross-reactive to all field strains. Another challenge is the relatively small number of mAb combinations that can be tested iteratively for therapeutic efficacy given the high cost and labor of *in vivo* virus challenge studies, especially when non-human primate (NHP) large animal model testing is needed. Therefore, for the rational development of antiviral therapeutic mAb cocktails it is important to implement approaches to identify combinations of mAbs with optimized molecular interactions in formulated cocktails, along with structural and functional analysis to define features that mediate efficient protection by these mAbs.

In this study, we describe the design of a cooperative two-antibody cocktail possessing neutralizing activity against the primary ebolaviruses that are responsible for outbreaks in humans—Ebola (EBOV), Bundibugyo (BDBV), and Sudan (SUDV) viruses (Kuhn, 2017). EBOV causes a severe disease in humans with 25% to 90% case fatality rates and significant epidemic potential. The largest epidemic to date occurred in 2013–2016 in West Africa with a total of 28,646 cases of Ebola virus disease (EVD) and 11,323 deaths reported (Coltart et al., 2017). This and the new ongoing outbreak in the Democratic Republic of the Congo (DRC) (CDC, 2019) highlighted the need to accelerate development of EVD therapeutics (Park et al., 2015; Urbanowicz et al., 2016). The ebolavirus envelope (E) contains a single surface protein, the glycoprotein (GP), which is the major target for neutralizing mAbs (Lee and Saphire, 2009). We conducted analysis of >1,800 human mAbs against the GP and identified two classes of broadly reactive mAbs that cooperate for binding to the GP and neutralization of the virus. High-resolution structures illuminated a mechanism of cooperativity. The two-antibody cocktail offered protection in mice against the most antigenically divergent virus SUDV and demonstrated high therapeutic efficacy against live EBOV challenge in NHPs. These findings offered a rational strategy for development of a potent two-antibody cocktail design based on structural features of mAb interactions with ebolavirus GPs.

RESULTS

Identification and Functional Properties of Candidate Cocktail Human mAbs

Our previous work identified two potent therapeutic candidate mAbs EBOV-515 (immunoglobulin G1 [IgG1] subclass) and EBOV-520 (IgG4 subclass) from the B cells in human survivors of EVD. Each of these mAbs binds to a conserved epitope on the base of the GP, neutralizes all three ebolaviruses causing the disease in humans (EBOV, SUDV, and BDBV), protects mice challenged with EBOV, and offers partial protection against BDBV and SUDV (Gilchuk et al., 2018). This work also revealed the class of non-competing, glycan-cap-region-specific mAbs that enhance binding of EBOV-515 and EBOV-520 to the GP in a cooperative manner (Gilchuk et al., 2018), suggesting a strategy for two-antibody cocktail design. Here, we screened >1,800 GP-reactive human mAbs and identified two previously described glycan-cap-specific EBOV-437 and EBOV-442 (Gilchuk et al., 2018) and one additional mAb EBOV-548 (all IgG1 originally) as suitable partners to EBOV-515 or EBOV-520 for the design of cooperative two-antibody cocktail (Figures S1A–E; Table S1). Partner candidate mAbs were filtered on the basis of (1) neutralizing activity against wild-type (WT) ebolavirus (EBOV at least); (2) broad reactivity to EBOV, BDBV, and SUDV GPs; (3) cooperative enhancement of EBOV-515 and EBOV-520 binding to the EBOV GP; and (4) capacity to protect against EBOV challenge in mice.

Because of the potential utility of these mAbs as components of a therapeutic cocktail, we sought to characterize in depth the cooperative effects mediated by combinations of two mAbs. As the first partner of the cocktail, we chose the most well-characterized base-region-specific mAb EBOV-520. We expressed the variable gene sequences for this mAb in Chinese hamster ovary (CHO) cells as a recombinant IgG1-LALA Fc mutant molecule (rEBOV-520 LALA, or rEBOV-520) to diminish Fc effector function. rEBOV-520 LALA possessed the highest protective efficacy with low-dose treatment against EBOV in mice (Kuzmina et al., 2018) and acted principally via neutralization to protect against EBOV (Gilchuk et al., 2018). The second cocktail partner, mAb EBOV-548, potently neutralized EBOV and showed the highest activity of three identified cooperative glycan-cap-specific mAbs in a cooperative binding to the GP with rEBOV-520 as a partner mAb. EBOV-548 was produced as a functionally competent IgG1 (designated here as rEBOV-548 IgG1 or rEBOV-548), because engagement of the Fc region might be important for protection by the GP glycan-cap-specific mAbs (Gunn et al., 2018).

To assess the Fc-mediated killing of antigen-expressing cells by engineered variants of EBOV-520 and EBOV-548, we used a stably transfected EBOV-GP-expressing SNAP-tagged 293F cell line as a target and heterologous human peripheral blood mononuclear cells (PBMCs) as a source of effector cells. The SNAP-tag is a self-labeling protein tag that allows specific labeling of a target cell line with fluorescent dye, facilitating detection of effector-cell-mediated killing activity by flow cytometry (Domi et al., 2018). rEBOV-520 LALA showed low cytotoxic activity when compared with that of the control rEBOV-520 WT IgG1. rEBOV-548 IgG1 mediated efficient cell killing that was comparable to that of a recombinant form of a

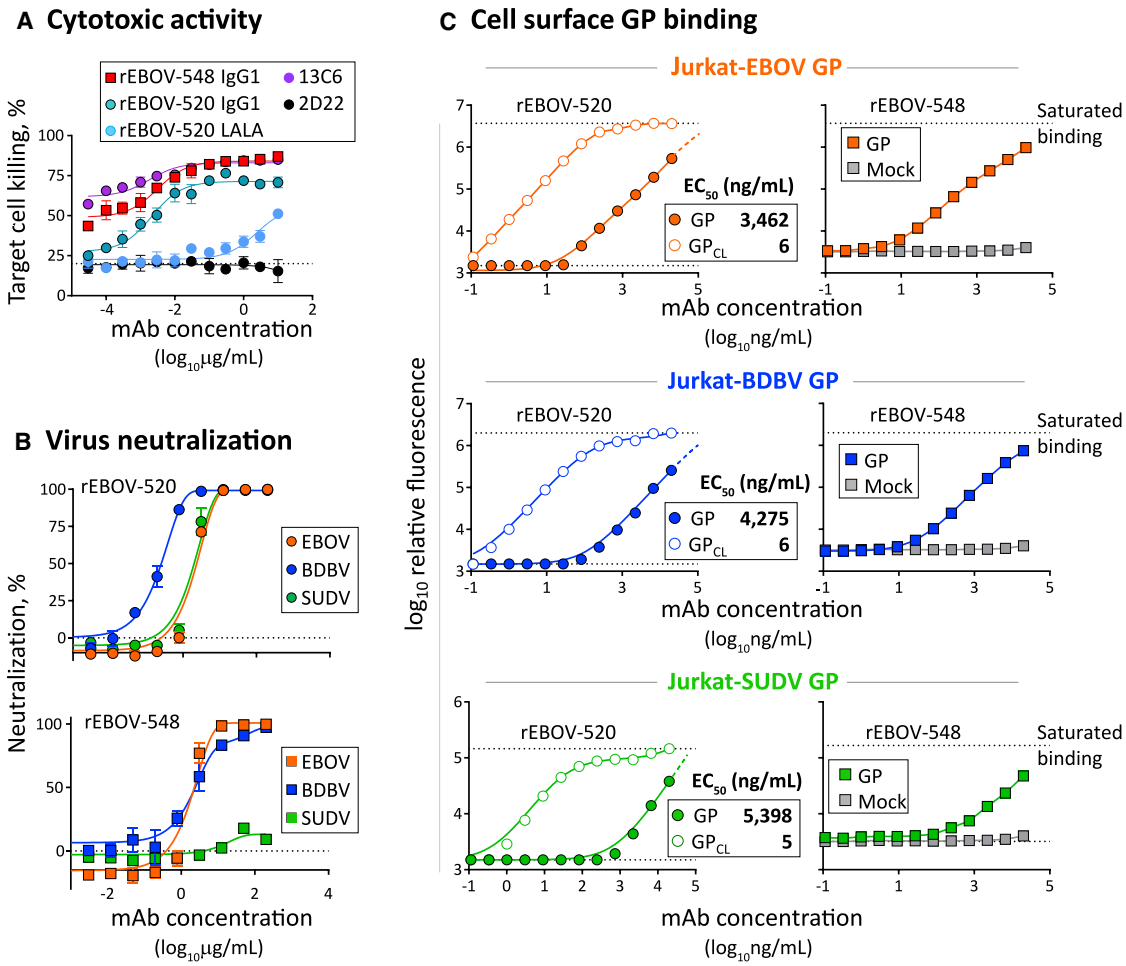

Figure 1. Candidate Cocktail Human mAbs rEBOV-520 and EBOV-548 Exhibit Differential Fc-Mediated Activities, Broadly Neutralize ebolaviruses, and Differentially Recognize the GP

(A) *In vitro* killing capacity curves for IgG1-engineered variants of mAbs determined using SNAP-tagged EBOV GP-expressing 293F cell line as a target and human PBMCs as source of effector cells. The dotted line indicates assay background.

(B) EBOV, BDBV, or SUDV neutralization. Viruses encoding enhanced green fluorescent protein (eGFP) were incubated with increasing concentrations of purified mAbs and infection was determined at 3 days after inoculation by measuring eGFP fluorescence in cells.

(C) Binding of candidate mAbs to intact cell-surface-displayed EBOV GP (solid shapes) or cleaved EBOV GP_{CL} (open shapes). Fluorescently labeled mAbs were incubated with a suspension of cells from a Jurkat cell line that was stably transduced with EBOV GP (Jurkat-EBOV GP), or the same cells treated with thermolysin to cleave GP (Jurkat-EBOV GP_{CL}); binding was assessed by flow cytometry. Dotted lines (black) indicate a dynamic range of mAb binding to the GP. Dashed lines show estimated curve slopes based on a constraint for saturating binding values. Mean ± SD (n = 3) from at least two independent experiments are shown in (A) to (C).

See also Figure S1 and Table S1.

glycan-cap-directed mAb c13C6, which is included in the ZMapp™ cocktail (Figure 1A) (Davidson et al., 2015). Similar functional profiles of these two mAbs were obtained using bead- or solid-phase-immobilized GP ectodomains and various human effector cells (Figures S1A and S1C). These findings confirmed the relatively high capacity of rEBOV-548 IgG1 to engage the Fc and diminished Fc function of rEBOV-520 LALA. All our next studies utilized these two Fc forms of rEBOV-520 and rEBOV-548.

We next assessed neutralizing activity of individual mAbs. rEBOV-520 potently neutralized all three ebolaviruses, whereas rEBOV-548 potently neutralized only EBOV and BDBV (Figures 1B and S1A). However, both mAbs were broadly reactive, as measured by binding to recombinant GP ectodomains or binding to full-length EBOV, BDBV, or SUDV GPs displayed on the surface of stably transduced Jurkat cell lines (Figures 1C, S1A, and S1B). We then tested mAb binding to each of the three Jurkat GP cell lines after treatment with thermolysin to mimic endosomal cathepsin cleavage to create a membrane-displayed cleaved GP (GP_{CL}). rEBOV-520 bound weakly to the intact GP but strongly to the GP_{CL}, demonstrating a saturable dose-response curve and ~500- to ~1,000-fold increase in binding to the GP_{CL} over the intact GP (Figure 1C). More efficient binding to the GP_{CL} was concordant with higher neutralizing activity of EBOV-520 against the virus displaying the EBOV GP_{CL} than the virus with the intact EBOV GP that we described in a previous

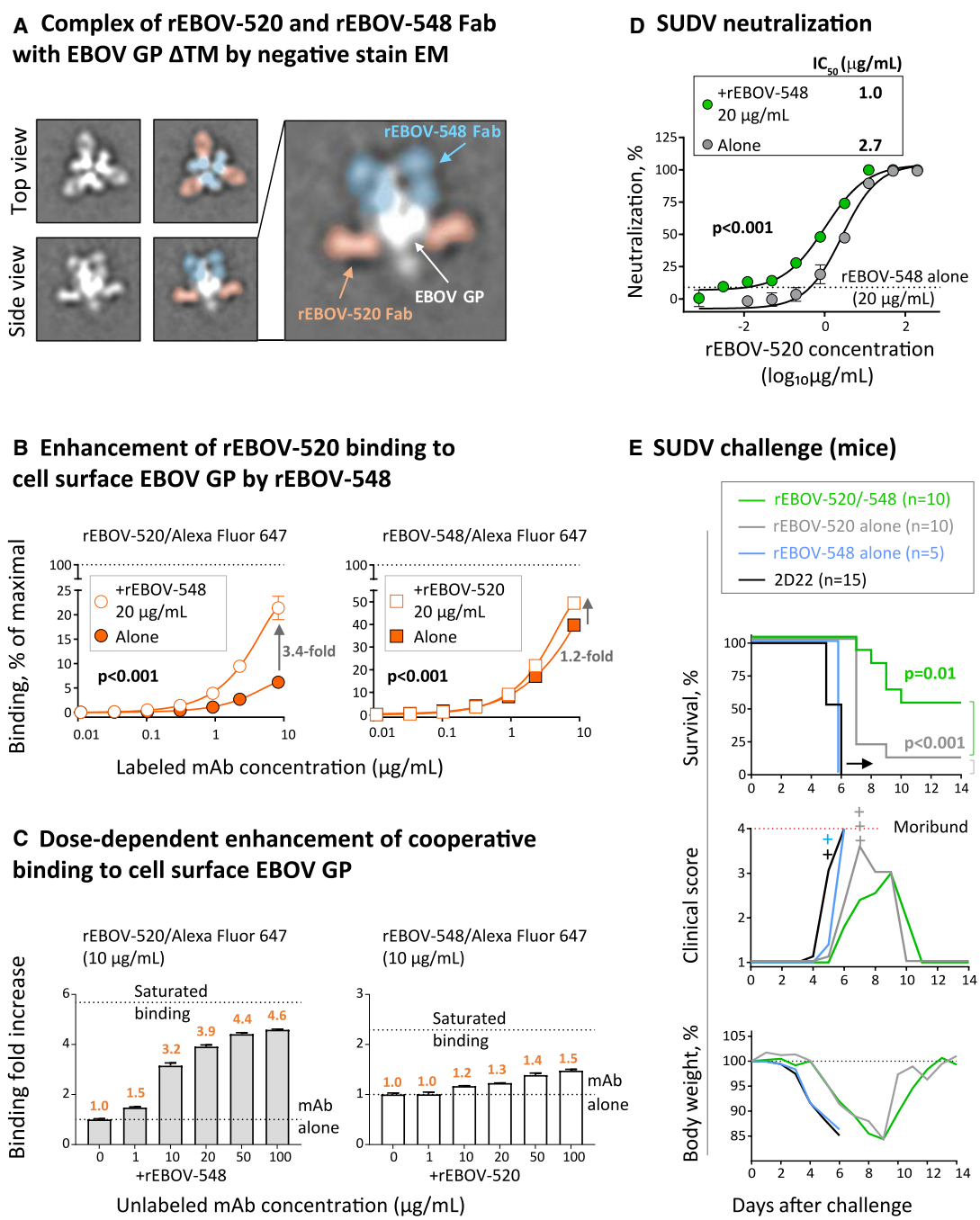

Figure 2. MAbs in the Cocktail Cooperate, Enabling Enhanced GP Binding, Virus Neutralization, and *In Vivo* Protection

(A) 2D class averages of Fab-EBOV GP complexes by negative stain EM demonstrate simultaneous binding of rEBOV-520 (orange) and rEBOV-548 (blue) to the GP.

(B) Binding to the Jurkat-EBOV GP was assessed by flow cytometry using Alexa Fluor 647 (AF647)-labeled mAb rEBOV-520 or rEBOV-548 alone (solid shape), or AF647-labeled mAb titrated into a fixed concentration (20 μg/mL) of unlabeled partner mAb (open shape) as indicated. Saturated binding was estimated as in Figure 1C. Effect from mAb composition was assessed by two-way ANOVA. Arrows show comparisons to estimate fold-increase in binding.

(C) Concentration-dependent potentiation of GP binding by partner mAb was assessed as in (B) using a single concentration of labeled mAb alone or the same labeled mAb in the mixture with increasing concentrations of unlabeled partner mAb as indicated. Fold increase in binding to the GP is shown with numbers in orange.

(D) rEBOV-548 potentiated neutralization of SUDV by rEBOV-520. Virus was incubated with increasing concentrations of rEBOV-520 alone (gray), or rEBOV-520 titrated into a sub-neutralizing concentration (20 μg/mL) of rEBOV-548 (green). Percent SUDV neutralization by rEBOV-548 alone is shown with dotted line. p value was estimated from a comparison of IC_{50} values (Student's t test).

(legend continued on next page)

study (Gilchuk et al., 2018). The glycan-cap-specific rEBOV-548 bound moderately and less efficiently to intact cell-surface-displayed GPs when compared with its binding to recombinant GPs (Figures 1C and S1B). Together, these results defined binding and functional features of the cocktail candidate mAbs and showed that the exposure of rEBOV-520 epitope is limited on the intact GPs of all three ebolaviruses.

mAbs in the Cocktail Cooperate, Enabling Enhanced GP Binding, Virus Neutralization, and *In Vivo* Protection

Negative stain electron microscopy (EM) analysis showed that rEBOV-520 and rEBOV-548 can bind to GPs simultaneously (Figure 2A). To characterize the cooperative effects of these two mAbs as a cocktail, we first assessed GP binding for each mAb in the presence or absence of the partner mAb. Fluorescently labeled rEBOV-520 or rEBOV-548 was titrated into a constant concentration of unlabeled partner mAb, as previously described (Gilchuk et al., 2018), and relative fluorescence from binding of the labeled mAb to the intact cell-surface-displayed EBOV, BDBV, or SUDV GP was determined. At a constant concentration of 20 μg/mL, rEBOV-548 enhanced binding of rEBOV-520 to the GPs of all three ebolaviruses 2- to 3-fold when compared with binding of rEBOV-520 alone. The cooperativity was mediated by rEBOV-548, because rEBOV-520 had a minor effect on binding of rEBOV-548 to the GP (Figure 2B). Cooperative binding of rEBOV-520 to the intact homologous EBOV GP increased steadily with increased concentrations of rEBOV-548 and up to ~5-fold higher than rEBOV-520 alone (Figure 2C), indicating that a higher dose of rEBOV-548 would be necessary to leverage strong cooperative effect in a two-antibody cocktail. Binding of rEBOV-520 to the intact GP in the cocktail did not fully match the strong saturating binding of rEBOV-520 by itself to the proteolytically primed GP_{CL} (Figure 2C). Therefore, binding of rEBOV-548 only partially enhanced accessibility of the base epitope on the intact GP for recognition by rEBOV-520, compared with the accessibility to the epitope on GP_{CL}.

We next assessed whether cooperative binding conferred an enhanced neutralizing activity to the cocktail by using first the most antigenically divergent virus, SUDV. rEBOV-548 itself did not fully neutralize SUDV, and rEBOV-520 neutralized SUDV, but with modest potency (Figure 1B and S1A). Consistent with the observed increase in cooperative binding of the SUDV GP (Figure S2A), rEBOV-548 at a sub-neutralizing concentration potentiated the neutralizing activity of rEBOV-520 against chimeric virus displaying the SUDV GP by reducing the half-maximal inhibitory concentration (IC_{50}) value by ~3-fold (Figure 2D). Neutralization by the cocktail was synergistic, as determined by the Chou and Talalay method that estimates the combination index (CI) to define the effect of drug combination: additive effects (CI = 1), synergism (CI < 1), and antagonism (CI >1) (Chou, 2010). We also demonstrated synergy in neutralization of the virus with the homologous EBOV GP using the cocktail (a 1:1 mixture of rEBOV-520 and rEBOV-548) (Figures S2B and S2C). Together, these data supported our finding for cooperative binding of rEBOV-520 and rEBOV-548 to the GP.

We next tested whether rEBOV-548 potentiated protection by rEBOV-520 in the cocktail against SUDV *in vivo* by using a stringent *Stat1*-deficient ($Stat1^{-/-}$) mouse challenge model that provides a uniform lethality (Raymond et al., 2011). An irrelevant mAb DENV 2D22 (IgG1 isotype) specific to the dengue virus E protein (Fibriansah et al., 2015) was used as a control. All SUDV-challenged mice that were treated with 10 mg/kg of rEBOV-548 mAb alone (which does not neutralize SUDV) on day 1 after infection succumbed to the disease by day 6 after infection, similarly to the animals in the control group. Treatment with rEBOV-520 alone delayed mortality; however, only 10% of animals survived. Treatment with the cocktail (a 1:1 mixture of rEBOV-520 and rEBOV-548) conferred higher protection, with 50% of animals surviving and an associated p value = 0.01 (Mantel-Cox test) when compared with the treatment with rEBOV-520 alone (Figure 2E). These results showed that rEBOV-548 complemented the activity of rEBOV-520 against SUDV *in vivo*. It is unknown whether protection in this model can predict protection against SUDV in NHPs.

Use of antibody cocktails is attractive because this approach avoids the high risk of virus escape by this RNA virus that is inherent in monotherapy approaches. We hypothesized that the cocktail of rEBOV-520 and rEBOV-548 counteracts the escape more efficiently than individual mAbs do because each mAb possesses independent neutralizing activity (EBOV and BDBV at least) and together they exhibit an enhanced activity. We used high-throughput and quantitative real-time cell analysis assay (RTCA) that measures virus-induced cytopathic effect to screen for escape mutations in the presence of individual mAbs or the cocktail (Figures S2D and S2E). Recombinant vesicular stomatitis viruses (rVSVs) displaying the EBOV GP (rVSV/EBOV GP) or SUDV GP (rVSV/SUDV GP) were incubated in the presence of increasing mAb concentrations, and we assessed neutralization in repeated passages in Vero cell monolayer cultures. Viruses escaping neutralization were assessed for susceptibility to neutralization by individual mAbs or the cocktail, and the genes encoding the GP were sequenced to confirm the presence of an escape mutation. Fifteen consecutive passages identified two rVSV/EBOV GP mutants that escaped neutralization by rEBOV-548 and one rVSV/SUDV GP mutant that escaped neutralization by rEBOV-520. Each of the mutants that we detected was selected in the presence of an individual mAb, and the mutations identified were within the predicted epitope for the respective mAb (Table S2). Virus escape was not detected in passages in the presence of the cocktail, as confirmed by neutralization of the late passage

(E) Cooperative enhancement of protection against SUDV infection in mice by rEBOV-548. $Stat1^{-/-}$ mice were inoculated with WT SUDV and treated at 1 dpi with 10 mg/kg rEBOV-520 alone, 10 mg/kg of rEBOV-548 alone, 20 mg/kg rEBOV-520/rEBOV-548 cocktail (1:1 mixture of each mAb), or mAb DENV 2D22 (control). Survival (top), combined clinical scores (middle), and combined body weights (bottom) of surviving mice are shown. Indicated groups were compared using Mantel-Cox test. A "+" indicates an animal found dead prior to reaching the pre-determined clinical score. Data are pooled from two to three independent experiments.

Mean ± SD (n = 3) from at least two independent experiments are shown in (B)–(D).

See also Figure S2 and Table S2.

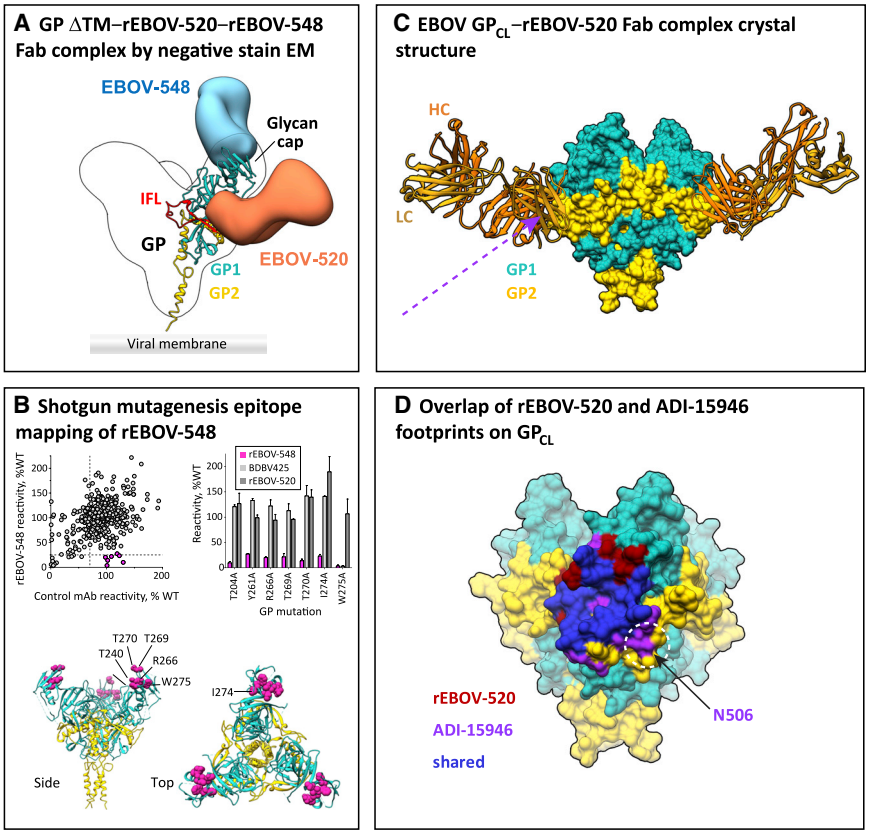

Figure 3. The Cocktail mAbs Recognize Relatively Conserved Epitopes on the Glycan Cap and Base Regions of the GP

(A) Negative stain EM reconstruction of rEBOV-548 Fab was overlaid onto a reconstruction of rEBOV-520 (EMDB-7955). A single protomer of EBOV GP is shown fit into GP density (Protein Database [PDB]: 5JQ3).

(B) Mutations to alanine in indicated residues that reduced EBOV-548 binding (< 25% of binding to WT EBOV GP, magenta bars) but did not affect binding of control mAbs BDBV425 or rEBOV-520 (gray bars) were identified (top). The exception is the W275A mutation that reduced binding of BDBV425, because W275 is part of the BDBV425 epitope on the GP. Error bars represent the mean and range (half of the maximum minus minimum values) of at least two replicates. Identified epitope residues are shown on EBOV GP trimer (PDB: 5JQ3) in magenta (bottom).

(C) Crystal structure of EBOV GP$_{CL}$ in complex with rEBOV-520 Fab. EBOV GP$_{CL}$ is shown in surface representation. GP1 colored in cyan and GP2 colored in yellow. rEBOV-520 Fab is shown in cartoon representation. The heavy chain (HC) colored dark orange and the light chain (LC) colored light orange. The approach angle of ADI-15946 is indicated with a violet dashed arrow.

(D) The footprints of rEBOV-520 or ADI-15946 Fab on EBOV GP$_{CL}$ (represented as in C) are shown in red or violet, respectively. Their shared footprint is shown in blue. The location of the non-conserved EBOV GP residue N506 is indicated within a dashed white circle.

See also Table S3.

viruses with individual mAbs rEBOV-520 or rEBOV-548. The rVSV/EBOV GP mutants that escaped neutralization by rEBOV-548 that we isolated were neutralized fully by rEBOV-520 alone and by the cocktail, showing that if one neutralizing mAb loses activity because of a virus variant with an escape mutation, the other neutralizing mAb in the cocktail maintained activity (Table S2). These data strongly suggest that the use of this cocktail enhances the effective neutralizing potency of the mAbs and counteracts virus escape of the homologous EBOV. Although escape was not detected with the cocktail, the rEBOV-520 escape mutant we identified for rVSV/SUDV GP (N514Y, a conserved residue for EBOV, BDBV, and SUDV GP) was not fully neutralized by either mAb rEBOV-548 alone or by the cocktail, suggesting the possibility of escape by the heterologous SUDV.

Therefore, cooperativity in GP binding by the cocktail could benefit therapeutic effectiveness by enhancing virus neutralization, enhancing *in vivo* protection, and reducing the risk of virus escape.

The Cocktail mAbs Recognize Relatively Conserved Epitopes of Two Major Antigenic Sites of the GP

We previously reported negative stain EM reconstructions of EBOV-520 in complex with the GP (Gilchuk et al., 2018). The epitope of EBOV-548 has not yet been characterized. We performed negative stain EM studies by using complexes of rEBOV-548 Fab alone or a combination of both rEBOV-548 and rEBOV-520 Fabs with recombinant trimeric EBOV GP ΔTM. rEBOV-548 recognized the glycan cap region and bound nearly perpendicular to the surface of the GP (Figure 3A), similar to the binding pose of c13C6, but also made interactions with the interior of the chalice within the outer domain of the glycan cap. c13C6, however, does not enhance rEBOV-520 binding, whereas rEBOV-548 does (data not shown).

To define key contact residues of the epitope, we used alanine scanning mutagenesis of the GP and tested the binding of rEBOV-548 to individual members of a shotgun mutagenesis alanine mutation library of the EBOV GP displayed in cells. We also generated antibody escape mutant EBOV viruses and determined their GP sequence. Mutations T240A, Y261A, R266A, T269A, T270A, I274A, and W275A reduced binding to the GP (Figure 3B), and escape mutation L273P reduced neutralizing potency. The key contact residues were positioned on the top of the glycan cap and within a region with relatively low sequence conservation. However, five of seven contact residues were conserved among EBOV, BDBV, and SUDV GPs (EBOV GP residues Y261 and R266 are non-conserved) that explained broad reactivity of rEBOV-548. Together, these studies identified a site of vulnerability for antibody recognition on the glycan cap that mediated cross-reactivity and cooperative binding in the cocktail of rEBOV-548 and rEBOV-520.

We next defined the structural determinants of GP binding and reactivity breadth for rEBOV-520 by resolving the crystal structure of rEBOV-520 Fab in complex with EBOV GP$_{CL}$ to 3.46 Å resolution (Table S3). The rEBOV-520 Fab bound to the

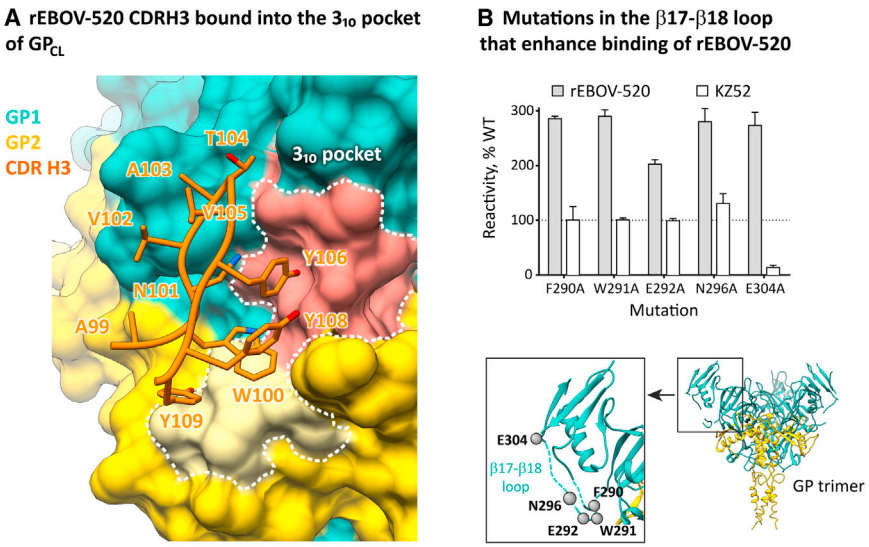

Figure 4. The Binding Site of rEBOV-520 Includes the 3_{10} Pocket That Is Fully Exposed in GP_{CL} but Masked by the β17-β18 Loop in Intact GP

(A) An enlarged view showing occupation of the 3_{10} pocket of the GP by rEBOV-520 CDRH3 residues. Ten residues of the CDRH3 tip are shown in orange cartoon. EBOV GP_{CL} is shown in surface representation with GP1 in cyan and GP2 in yellow. The 3_{10} pocket residues involved in the interface with rEBOV-520 CDRH3 and that showed a decrease in hydrogen-deuterium binding to the uncleaved GP as determined by HDX-MS, are mapped onto the surface of GP1 (light red) and GP2 (light yellow).

(B) Individual alanine mutation of six residues in the β17-β18 loop that increased binding by mAb EBOV-520 (gray bars) but did not affect binding of a recombinant form of the GP base mAb KZ52 (white bars) were identified (top). Mean and range (half of the maximum minus minimum values) of at least two replicate data points are shown. Positions of identified residues in the β17-β18 loop (green) are shown on EBOV GP (PDB: 5JQ3) with gray spheres (bottom).

See also Figure S3.

base of each protomer of GP_{CL}, and the constant domains were oriented upward from the viral membrane (Figure 3C). The rEBOV-520 footprint includes relatively conserved regions including the internal fusion loop (IFL) stem of the GP2 subunit and the hydrophobic pocket formed by five residues of the GP1 subunit and termed previously the "3_{10}" pocket (Zhao et al., 2016; West et al., 2019). The footprint of rEBOV-520 is distinct from that of the previously described broad human base-specific mAb ADI-15878 (Murin et al., 2018; West et al., 2018) but is similar to the footprint of the potent human-base-specific mAb ADI-15946 (Figure 3D), which fully neutralizes EBOV and BDBV but not SUDV (Wec et al., 2017; West et al., 2019). Both ADI-15946 and rEBOV-520 bound to the 3_{10} pocket and IFL stem regions of the fusion loop, unlike human mAb ADI-15878, which binds to the hydrophobic loop end of the structure and bridges to a neighboring GP protomer (King et al., 2019). However, rEBOV-520 likely gained reactivity against SUDV by having a footprint slightly higher on the GP base than the ADI-15946, or a different angle of approach than that of ADI-15946, which was directed downward toward the viral membrane (Figure 3C), in contrast to ADI-15946, which is directed upward from the membrane (West et al., 2019). This footprint allowed the mAb to avoid contact with the non-conserved EBOV GP residue N506 (R506 in SUDV GP) in the interface with rEBOV-520 (Figure 3D)—a key contact residue for binding with complementarity determining region 3 of heavy chain (CDRH3) of ADI-15946 (West et al., 2019). Our findings highlighted the variability in epitopes of lead therapeutic candidate mAbs and identified rEBOV-520 as a distinct representative among the class of 3_{10} pocket-targeting mAbs with an extended activity against SUDV.

Cooperativity in the Two-Antibody Cocktail Is Mediated by Structural Remodeling of the GP Glycan Cap

Analysis of the rEBOV-520 Fab-GP_{CL} crystal structure identified 26 GP_{CL} residues in the interface with rEBOV-520 Fab, 16 located in GP1 (amino acid [aa] 70–78, 104, 106, 107, 134, 136, 137, and 139) and ten located in GP2 (aa 510–514, 516, 545–547, and 549). The 18-amino-acid-long CDRH3 interacted with a conformational epitope on the GP1-GP2 interface by making direct contacts with 13 GP1 (aa 70–78, 106, 107, 127, and 139) and 5 GP2 (aa 510–514) residues that are relatively conserved among EBOV, BDBV, and SUDV (Figure S3A). rEBOV-520 bound to the 3_{10} pocket of the GP_{CL} formed by GP1 residues 70–78 (all contacted with CDRH3) and GP2 residues 510–516 (four of seven contacted with CDRH3) that line the bottom part of the pocket (Figure 4A). In the unbound, full-length GP, the 3_{10} pocket normally is occupied by the flexible descending β17-β18 loop of the glycan cap (GP1 residues 287–291) that impedes access to the pocket. Like ADI-15946 (West et al., 2019), rEBOV-520 either bound to a conformation of GP in which the β17-β18 loop is displaced, or actively displaced it from the pocket upon binding. The loop is not present in the GP_{CL}, being removed by cleavage. We used hydrogen-deuterium exchange mass spectrometry (HDX-MS) to compare deuterium labeling of peptides generated after digestion of the GP and GP_{CL} with pepsin. Decrease in labeling of GP 3_{10} pocket residues involved in the interface with CDRH3 confirmed limited accessibility of rEBOV-520 epitope in a structure of intact GP trimer (Figure 4A and S3B). Cleavage removes the glycan cap with the β17-β18 loop and exposes the pocket, which explained enhanced binding of rEBOV-520 to GP_{CL} (Figure 1C) and enhanced neutralization potency of this mAb against virions bearing the GP_{CL} compared with intact GP (Gilchuk et al., 2018).

Previous work suggested that binding of the non-neutralizing macaque mAb FVM09 to the β17-β18 loop itself displaces the loop causing unmasking of the neutralizing epitopes for mAbs 2G4 and ADI-15946 on the GP base (Howell et al., 2017; West et al., 2019). However, unlike with FVM09,

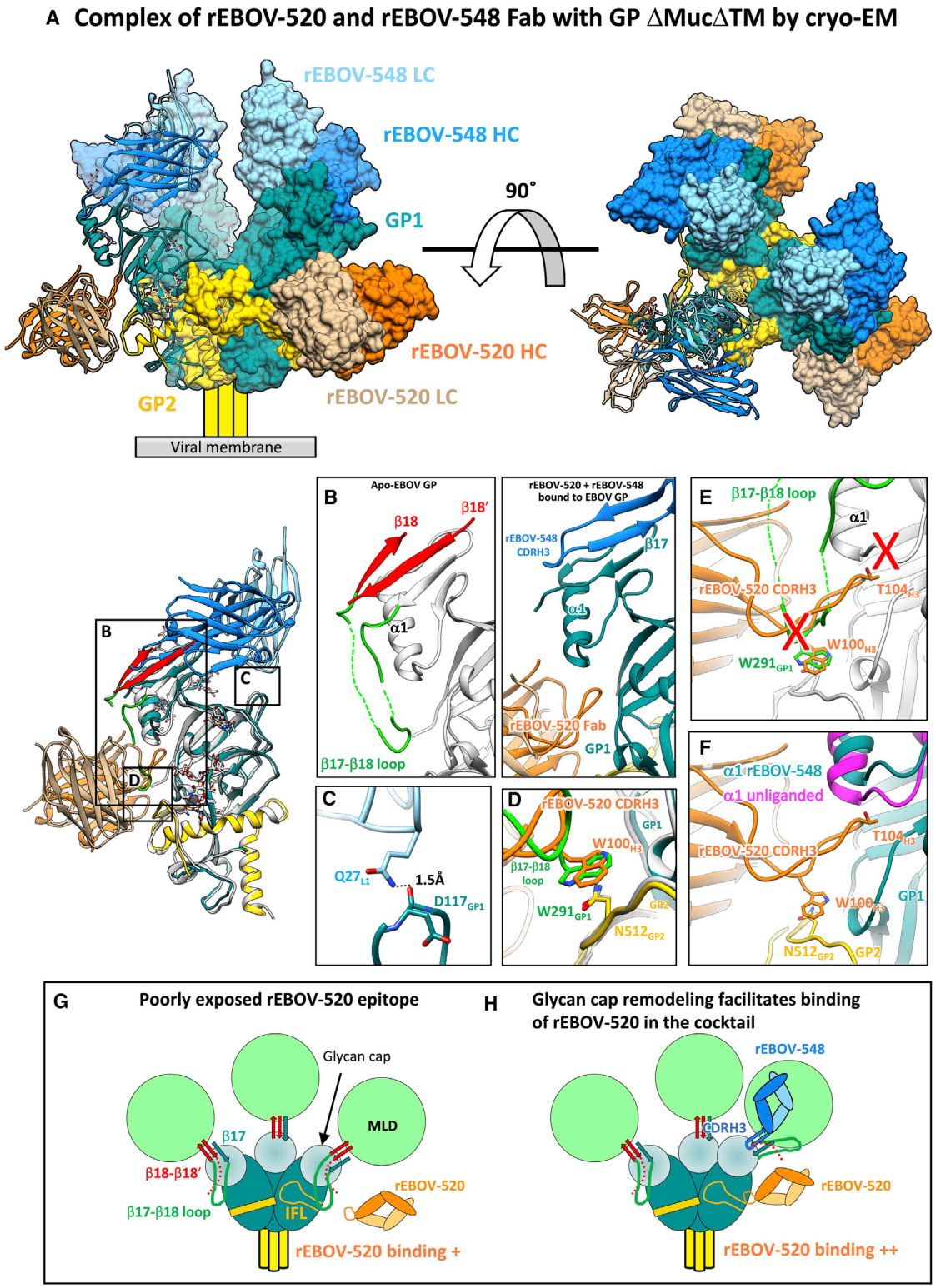

Figure 5. Cooperativity in the Cocktail of rEBOV-520 and rEBOV-548 Is Mediated by Structural Remodeling of the GP Glycan Cap

(A) Cryo-EM structure of EBOV GP ΔMucΔTM (GP1 in cyan and GP2 in yellow) bound to rEBOV-548 Fab (HC in dark blue and LC in light blue) and rEBOV-520 Fab (HC in orange and LC in tan). Shown is a side view (left) and top view (right) in relation to the viral membrane. Fab constant domains were excluded by masking. (B) The crystal structure of apo-EBOV GP ΔMucΔTM (PDB: 5JQ3) with the β18-β18′ region (red) and the β17-β18 loop (green). On the right is the EBOV ΔMucΔTM-rEBOV-520-rEBOV-548 cryo-EM structure; the rEBOV-548 CDRH3 loop is shown in blue.

(legend continued on next page)

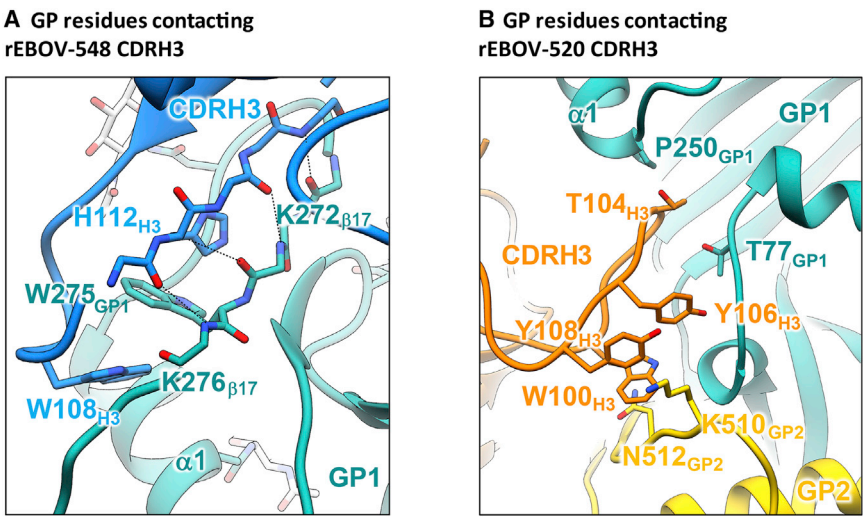

Figure 6. MAbs rEBOV-520 and rEBOV-548 Bind to the GP in a Manner That Mimics Interactions in Unliganded GP

(A) rEBOV-548 CDRH3 loop residues that make contacts along the β17 sheet in GP1 (from K272–K276), forming several hydrogen bonds within an extended beta sheet in the glycan cap (black dotted lines) and mimic this interaction by the β18-β18′ region in the unliganded structure are shown. Another key contact shown is with W275, which is cradled within a hydrophobic pocket formed by the tip of the CDRH3 at W108 and H112.

(B) Interaction of the rEBOV-520 CDRH3 loop residue W100 with the 3_{10} pocket residue N512 in GP1 that mimics interaction by the β17-β18 loop residue in the unliganded structure, and additional interactions when the glycan cap is intact (Y108 with K510 in GP2, Y106 with T77 and a hydrophobic patch in GP1, and T104 with the base of the α1 helix at P250 in GP1) are shown.

whose binding was fully abolished by several alanine mutations in the β17-β18 loop (Howell et al., 2017), none of the alanine mutations within the β17-β18 loop reduced rEBOV-548 binding to the GP (data not shown). Rather, alanine substitutions in several residues of the β17-β18 loop, which are distal to the rEBOV-548 epitope in the upper portion of the glycan cap, increased rEBOV-520 binding by ~1.6- to 3-fold compared with binding to the wild-type GP (Figure 4B). This suggested that rEBOV-548 does not bind to the β17-β18 loop, and binding to the loop itself is not required for cooperative enhancement of rEBOV-520 binding.

To determine the structural determinants of cooperativity within the cocktail, we solved a cryogenic EM (cryo-EM) structure of rEBOV-520 and rEBOV-548 Fab in complex with EBOV GP with the glycan cap intact and mucin-like domain-deleted (ΔMuc) at 4.1 Å resolution (Figure 5A; Table S4). To determine the contribution of rEBOV-548 to cooperativity, we also solved a cryo-EM structure of rEBOV-548 Fab alone in complex with EBOV GP ΔMuc at 4.0 Å resolution (Figure S4; Table S4). We were unable to solve the structure in the glycan cap region in the complex of GP-rEBOV-520 Fab alone by cryo-EM (data not shown), which is likely due to flexibility of the glycan cap.

Unlike the previously described mAb FVM09, our structure revealed that rEBOV-548 does not bind directly to the β17-β18 loop. Instead, the CDRH3 loop of rEBOV-548 directly interacted with the β17 strand (residues 272–275) of GP1, forming an extended beta sheet with the glycan cap, including highly conserved critical epitope residues I274 and W275 that were defined by loss of binding with alanine substitution and L273, for which mutation to proline resulted in loss of neutralizing activity. rEBOV-548, similarly to EBOV-442, inhibited glycan cap cleavage, which could be the molecular basis for neutralizing activity by these mAbs (Gilchuk et al., 2018). Two non-conserved GP1 residues Y261 and R266, whose mutation to alanine decreased binding of rEBOV-548 (Figure 3B), did not directly contact the rEBOV-548 paratope and were not within the cleavage site. In the SUDV GP, natural mutations Y261H and R266L affected rEBOV-548 activity in a similar way by lowering the EC_{50} for binding and reducing its neutralizing potency (Figures 1B, S1A, and S1B), suggesting destabilization of the epitope by these adjacent mutations. In both rEBOV-548 Fab alone and rEBOV-520 + rEBOV-548 Fab bound states, the β18-β18′ domain, C-terminal of the GP β17-β18 loop was displaced and structurally mimicked by the CDRH3 loop of rEBOV-548 (Figures 5B and S4). The rEBOV-548 LC contacted GP1 through hydrophobic interactions at the loop between α1 and β17 (residues 268 and 269) and through $Q27_{L1}$ contacting residue D117, making a possible H-bond with the backbone of D117 (Figure 5C) that anchors the mAb to the inner chalice of the GP (Figure 5A). We observed rEBOV-548-mediated destabilization and dissociation of the GP trimer (Figure S5A). Such a dissociation was limited in the presence of the stalk-specific mAb ADI-16061 that was used to stabilize the GP for cryo-EM with rEBOV-548. It is unclear whether this disruption seen with soluble GPs also occurs in membrane-anchored GPs or whether it contributes to the synergy. Analysis of rEBOV-520 interactions in the structure of rEBOV-520 + rEBOV-548 bound to the GP showed that the rEBOV-520 CDRH3 loop makes additional contacts beyond the 3_{10} pocket when the glycan cap is intact. These contacts include $Y108_{H3}$ with K510 in GP2, $Y106_{H3}$ with

(C) Interaction of the rEBOV-548 LC residue $Q27_{L1}$ with GP1 residue D117.

(D) Enlarged view of the rEBOV-520 epitope (orange, yellow, and cyan) overlaid with the unliganded structure of EBOV GP ΔMucΔTM (gray and green).

(E) The β17-β18 loop and the base of the α1 helix in the glycan cap present in the unliganded GP structure (gray and green) overlaid with rEBOV-520 bound GP structure (orange). The regions of interference with rEBOV-520 binding are shown with red crosses.

(F) The position of the α1 helix in the rEBOV-520-rEBOV-548 bound GP structure (cyan) overlaid with that of the unliganded GP helix (magenta).

(G and H) A cartoon of proposed cooperativity mechanism for the GP binding by the cocktail in which rEBOV-520 alone binds weakly (G), but in the presence of changes caused by rEBOV-548 engagement, rEBOV-520 binds strongly (H).

See also Figures S4–S6, Table S4, and Video S1.

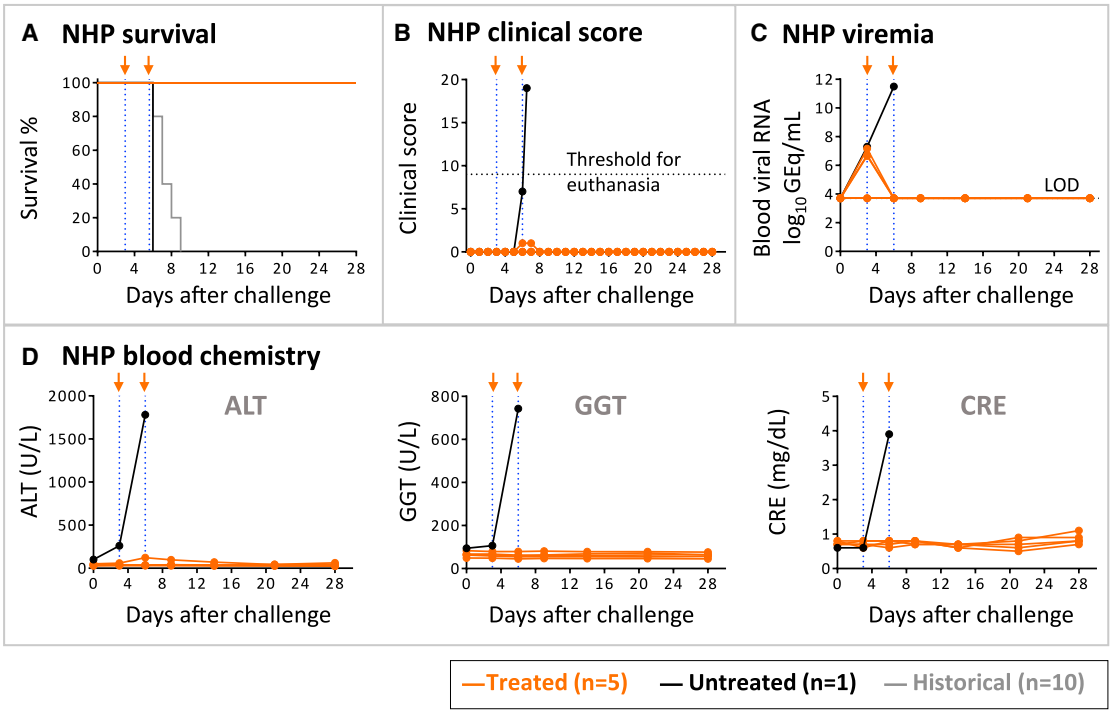

E Infectious virus load in various tissues

NHP ID	Treatment	Tissue	Viral load, log_{10}PFU per gram of tissue	Cytopathic effect	
			Intact	Passage 1	Passage 2
M1	Treated	Pancreas	<	<	<
		Brain	<	<	<
		Brain stem	<	<	<
M2	Treated	Eye	<	<	<
M3	Treated	Spleen	<	<	<
M4	Treated	Testis	<	<	<
M5	Treated	Spleen	<	<	<
C1	Untreated (control)	Liver	**7.4**	Not tested	
		Spleen	**7.3**		
		Eye	**5.9**		

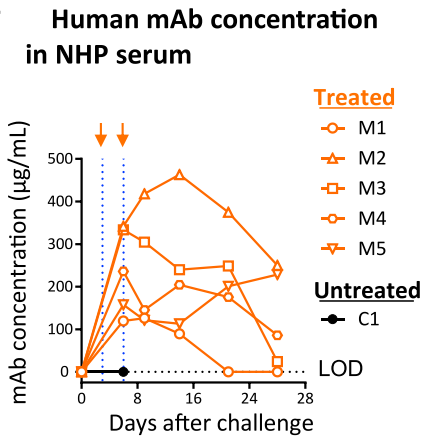

Figure 7. The mAb Cocktail Protects Nonhuman Primates against EVD

Animals received a lethal dose of the EBOV Kikwit isolate intramuscularly (i.m.) on day 0 and were treated with total 30 mg/kg of the cocktail (1:1 mixture of each mAb) intravenously on days 3 and 6 after infection (n = 5). The contemporaneous control was an untreated NHP challenged with the virus (n = 1). One experiment was performed.

(A) Kaplan-Meier survival plot.

(B) Clinical score.

(C) Kinetics of blood viral load as determined by qRT-PCR.

(D) Selected blood chemistry measurements. Abbreviations are as follows: ALT, alanine aminotransferase; GGT, gamma-glutamyl transpeptidase; CRE, creatinine.

(E) Plaque assay measurement of infectious virus load in various peripheral tissues of treated NHPs (day 28 after infection). Tissues from succumbed untreated NHP (day 6 after infection) used as a control. The < symbol indicates infections virus was not detected.

(F) Concentration of human mAbs that was determined in serum of five treated and one control NHPs at indicated time points after virus challenge. mAb treatment times are indicated with blue dotted lines and orange arrows.

(legend continued on next page)

T77 in GP1, and $T104_{H3}$ with P250 in the base of the α1 loop of GP1. The rEBOV-520 CDRH3 residue $W100_{H3}$ bound to N512 in GP2, displacing the β17-β18 loop and mimicking the N512 interaction with $W291_{GP1}$ of the β17-β18 loop in the unliganded structure (Figure 5D). Residues T77, K510, and N512 were highly conserved among EBOV, BDBV, and SUDV GPs. Of note, our previous study identified N512 as a key epitope residue for rEBOV-520, given that N512A mutation reduced binding to the GP (Gilchuk et al., 2018). Therefore, for efficient binding rEBOV-520 must overcome interference of the β17-β18 loop (at $W291_{GP1}$) and α1 helix (at $P250_{GP1}$) contained in the glycan cap structure (Figure 5E). When two Fabs of the cocktail bound to the GP, the β18-β18′ region is displaced and the glycan cap pulled back, along with the β17-β18 loop, to allow efficient binding of rEBOV-520 (Figure 5F). However, in a structure where rEBOV-548 bound to the GP alone, the glycan cap was not displaced to the degree it was when rEBOV-520 was bound but rather is reminiscent of the structure of unliganded GP. Although the β18 and β18′ strands are displaced and replaced by rEBOV-548 CDRH3, the β17-β18 loop is largely intact and bound to the base of the IFL, blocking the 3_{10} pocket (Figure S4). Comparing solvent exclusion, the unliganded GP and the GP in a complex with rEBOV-548 alone appeared very similar, except for in the β18-β18′ domain. Most of the region where the rEBOV-520 CDR3 bound was still excluded and the α1 helix was not displaced (Figure S5B), consistent with our observation that rEBOV-548 did not fully potentiate binding of rEBOV-520. These data suggested that in the cocktail, rEBOV-520 alone was largely responsible for complete displacement of the β17-β18 loop as well as displacing the α1 helix in the cocktail, whereas rEBOV-548 acted by displacement of the β18-β18′ domain and the C-terminal portion of the β17-β18 loop, alleviating structural and kinetic restraints for efficient rEBOV-520 binding (Figure S6).

We concluded that structural remodeling is the principal mechanism for the enhanced GP binding and ebolavirus neutralization by the cocktail of two cooperative, naturally occurring human mAbs rEBOV-548 and rEBOV-520 (Figures 5G, 5H, and S6; Video S1).

Analysis of the molecular interaction between rEBOV-520 and rEBOV-548 with the GP illustrated that both mAbs use molecular mimicry whereby CDRH3 binds to the GP in a manner analogous to the interactions in the unliganded GP. Thus, rEBOV-548 CDRH3 interfaced with the β17 sheet of the glycan cap and mimicked the interaction of the β18-β18′ region with the β17 sheet (Figures 5B and 6A), and rEBOV-520 CDRH3 interfaced with the 3_{10} pocket residues mimicking the interaction by the β17-β18 loop in the unliganded GP (Figures 5D and 6B). Together, these experiments defined key molecular features that mediate binding and cooperativity by the cocktail of two broadly neutralizing human mAbs.

The mAb Cocktail Protects Non-human Primates against EVD

We next used a NHP rhesus macaque EBOV challenge model, which recapitulates many key features of EVD in humans (Geisbert et al., 2015; Bennett et al., 2017), to determine the efficacy of treatment by the cocktail. Rhesus macaques were assigned to one treatment group of five animals. After intramuscular challenge with a lethal target dose of 1,000 plaque-forming units (PFU) of the Kikwit variant of EBOV, all NHPs of the treatment group received intravenously two 30 mg/kg doses of the cocktail (1:1 mixture of rEBOV-520 and rEBOV-548) spaced 3 days apart (days 3 and 6 after infection). An additional animal was studied as a contemporaneous control and was left untreated, along with ten historical untreated controls (7 days post-infection [dpi] median survival, inoculated by the same route with the same stock of virus). The control untreated animal developed a high clinical score and succumbed to the disease on day 6 after infection. The two-dose therapeutic cocktail treatment provided complete protection of NHPs from mortality and clinical signs of EVD (Figures 7A, 7B, and S7). Before the first treatment (day 3 after infection) three of five NHPs from the treatment-designated group and also the control untreated NHP developed detectable viremia; plasma titers ranged from 6.7 $\log_{10}$ to 7.3 $\log_{10}$ genome equivalents (GEQs) per mL, as measured by qRT-PCR (Figure 7C). The plasma titer of infectious virus that was assessed by plaque assay on day 3 after infection was below the limit of detection in all animals. However, by day 6 after infection, the viral load in all untreated animals, including in the NHP control from this study and in the historical controls, was as high as >5 $\log_{10}$PFU/mL or >11 $\log_{10}$ GEQ/mL (Figures 7C and S7). Concordant with full protection, by day 6 after infection all treated NHPs, including three registered as highly viremic on day 3 after infection, no longer had detectable viremia in the plasma. In various tissues harvested from treated animals on day 28 after infection, qRT-PCR analysis, which detects both infectious and non-infectious neutralized particles that have not yet been cleared, revealed virus, confirming active EBOV infection in all NHPs in the treatment group before treatment (Table S5). We next assessed changes in blood chemistries that are typically associated with EVD to further characterize the efficacy of the mAb cocktail treatment (Table S6). The liver enzymes alanine aminotransferase (ALT), gamma glutamyl transferase (GGT), and alkaline phosphatase (ALP), which are indicators of EVD, were elevated in untreated NHPs on day 6 after infection—the peak of viremia and the disease (Figures 7B and 7C). Treated animals did not show signs of acute liver injury on day 6 after infection or later time points, displaying low amounts of ALT, GGT, ALP when compared with those of untreated NHP (Figure 7D; Table S6). To probe the possibility of selection of escape mutants in the presence of the cocktail, we assessed several peripheral tissues for the presence of live infectious

Orange curves indicate treated and black curves indicate untreated animals in (A)–(D). Ten historical controls (gray) are shown for comparative purposes in (A). The black dotted line in (B) indicates the clinical score threshold for euthanasia. The black dotted line in (C) indicates the limit of detection (LOD) for genome equivalents (GEQ); each measurement represents the mean of technical duplicates.
See also Figure S7 and Tables S5 and S6.

virus to cover all NHPs and using a range of tissues that had the higher number of viral genomes detected by the qRT-PCR. All tested tissues from treated NHPs were confirmed to be negative for live virus on day 28 after infection, showing that the cocktail treatment provided sterilizing immunity (Figure 7E). Human IgG capture ELISA of serum samples revealed that circulating cocktail mAbs in the treated NHPs ranged from 125 to 460 μg/mL (Figure 7F). Given the relevance of such high mAb concentration for strong cooperative interactions (Figure 2C), cooperativity mediated by the cocktail likely contributed to the effectiveness of treatment.

In summary, the two-antibody cocktail that deploys multiple functions (a mechanism of neutralization for each of two mAbs, a synergy mediated by the cocktail, and Fc-mediated effector functions exhibited by rEBOV-548) demonstrated high potency to revert EVD in NHPs.

DISCUSSION

Here, we reported determinants of cooperativity for improved virus binding and neutralization in the cocktail. Our studies define essential features of cooperative mAbs with implications for the design of therapeutic cocktails: (1) we showed that mAbs enabling cooperative neutralization of ebolaviruses are generated by the immune response of human EVD survivors, (2) we identified epitopes for cooperative human mAbs, (3) we described remodeling of glycan cap structures of the GP as a mechanism of mAb cooperativity, (4) we identified molecular mimicry as a mechanism of ebolavirus GP recognition by human mAbs, (5) we showed that a cocktail of two cooperative human mAbs could mediate enhanced activity against heterologous ebolaviruses, (6) we demonstrated therapeutic effectiveness of a two-antibody cocktail in NHPs against EVD, (7) we identified Fc-effector function variants of the GP base- and glycan-cap-specific mAbs that mediate protection against EVD in NHPs.

To date, monotherapy treatment with mAb114 or treatment with two fully human mAb cocktails, REGN-EB3 or MBP134^{AF}, have been evaluated for clinical development. MBP134^{AF} is a two-antibody cocktail with pan-ebolavirus activity that demonstrated efficacy in NHPs (Bornholdt et al., 2019). REGN-EB3 is a three-antibody cocktail (Pascal et al., 2018), and mAb114 is a single mAb that is specific to the receptor binding site of the GP (Corti et al., 2016a)—both are monospecific to EBOV. REGN-EB3 and mAb114 were recently assessed in the field in the DRC outbreak of human EVD, and early treatment was associated with reduction of the mortality rate to 6% with REGN-EB3 or to 11% with mAb114 (Nature News, 2019). mAb114 is the only EBOV antibody described that has been shown so far to protect NHPs in monotherapy settings. Even so, the protection mediated by the cocktail of mAb114 + mAb100 was better than that mediated by mAb114 alone (Corti et al., 2016a). In the cocktail, there is also the potential benefit of avoiding the high risk of virus escape that is inherent in monotherapy approaches. Targeting cross-reactive epitopes might be another approach to reduce the viral escape, given that conserved regions are more likely to be critical for the virus function. Therefore, having a single broad cocktail that is at least as effective as the existing monospecific cocktail against EBOV would be practical. The cocktail of rEBOV-520 and rEBOV-548 was formulated to add a principle of cooperativity (e.g., incorporation of a pair of non-competing and potently neutralizing mAbs that together exhibit an enhanced activity). Therefore, in addition to the reactivity breadth that extended to BDBV and SUDV, the cocktail of rEBOV-520 and rEBOV-548 incorporated four principal activities against homologous EBOV: the independent neutralizing activities of (1) rEBOV-520 and (2) rEBOV-548, (3) an enhanced combined activity because of synergy in the cocktail, and (4) Fc-mediated effector function by rEBOV-548. A comparison to the historical NHPs studies with REGN-EB3, mAb114, and MBP134^{AF} qualifies the cocktail of EBOV-520 and EBOV-548 as highly protective against EBOV. The next studies should determine whether this cocktail protects NHPs against heterologous ebolaviruses.

The mAbs in the cocktail of rEBOV-520 and rEBOV-548 can act by several mechanisms. The GP binding studies demonstrated that the strongest enhancement by rEBOV-548 in the cocktail is achieved at higher mAb concentrations. Given the relatively high concentration of circulating mAbs after intravenous administration of IgG in treated NHPs, we suggest that enabled cooperativity is one of the mechanisms that likely contributed to the effectiveness of treatment, along with virus neutralization and Fc-mediated function.

Individual mAbs of the rEBOV-520 and rEBOV-548 cocktail potently neutralized EBOV and BDBV. Therefore, unlike with non-neutralizing synergistic mAb FVM09 (Howell et al., 2017), synergy is added but not a necessary feature to achieve neutralization by the cocktail of rEBOV-520 and rEBOV-548. Synergistic cocktail formulated with two neutralizing mAbs would likely be more efficient to counteract viral escape.

Cooperativity in the cocktail of rEBOV-520 and rEBOV-548 is mediated by recognition of the glycan cap epitope and conformational epitope spanning GP1 and the IFL of GP2. Several studies identified the IFL as a site of vulnerability for potent mAbs that can act solely by neutralization to protect (Gilchuk et al., 2018; Wec et al., 2017). MAbs recognizing glycan cap epitopes have been considered as inferior for therapeutic development because of possible cross-reactivity with soluble GPs (sGPs) (Mohan et al., 2012). Recent studies, however, suggested an indispensable role for Fc-mediated effector functions in the protection against EBOV by glycan-cap-specific mAbs (Gunn et al., 2018). It was unknown whether these functions (e.g., neutralizing activity and Fc engagement) in the cocktail of these two mAb specificities were essential and sufficient for efficacy in NHPs. Our study suggested that both functions could be important for virus control and EVD prevention by showing that the cocktail of the Fc-function-competent IgG1 form of glycan-cap-specific rEBOV-548 and functionally impaired IgG1-LALA form of neutralizing IFL-specific rEBOV-520 mediated therapeutic protection in NHPs.

The key structural aspect of this work is the finding that remodeling of the glycan cap is necessary for efficient binding of potent mAb rEBOV-520 to a vulnerable epitope on GP2, and this remodeling is facilitated in the presence of the GP1-specific mAb rEBOV-548. Therefore, this work defines

cooperative interactions between mAbs of the two major epitope specificities for GP recognition, and unveils cooperative binding of the GP as a mechanism for the enhanced ebolavirus neutralization and protection. Principles of mAb-antigen interactions demonstrated here with ebolavirus could aid in the design of therapeutic cocktails against other viral targets.

STAR★METHODS

Detailed methods are provided in the online version of this paper and include the following:

- KEY RESOURCES TABLE
- LEAD CONTACT AND MATERIALS AVAILABILITY
- EXPERIMENTAL MODEL AND SUBJECT DETAILS
  - Human samples
  - Cell lines
  - Viruses
  - Mouse models
  - NHP model
- METHOD DETAILS
  - Generation of human B cell hybridomas producing mAbs
  - Screening strategy to identify partner mAbs for therapeutic cocktail
  - mAb isotype and gene sequence analysis
  - mAb production and purification
  - GP expression and purification
  - ELISA binding assays
  - Kinetics of mAb binding analysis by biolayer interferometry (BLI)
  - Cell surface displayed GP mAb binding
  - Cooperative binding to cell surface displayed GP
  - Epitope mapping using an EBOV GP alanine-scan mutation library
  - Generation of virus neutralization escape mutants
  - Neutralization assays
  - Real-time cell analysis assay (RTCA)
  - Rapid fluorometric antibody-mediated cytotoxicity assay (RFADCC)
  - Antibody-mediated cellular phagocytosis by human monocytes (ADCP)
  - Antibody-mediated neutrophil phagocytosis (ADNP)
  - Antibody-dependent NK cell activation
  - Mouse challenge
  - NHP challenge
  - Detection of virus load by plaque assay or quantitative reverse transcription PCR analysis (qRT-PCR)
  - NHP serum biochemistry
  - Detection of circulating human mAbs in NHP serum
  - Single particle negative stain electron microscopy
  - Single particle cryogenic electron microscopy
  - Epitope mapping using peptide fragmentation and hydrogen-deuterium exchange mass spectrometry (HDX-MS)
  - Crystallography and structure determination
- QUANTIFICATION AND STATISTICAL ANALYSIS
- DATA AND CODE AVAILABILITY

SUPPLEMENTAL INFORMATION

Supplemental Information can be found online at https://doi.org/10.1016/j.immuni.2020.01.001.

ACKNOWLEDGMENTS

We thank J. Slaughter, C. Schoeder, N. Kose, S. Smith, K. Schey, W. White, J.D. Laughlin, J. Geisbert, K. Agans, D. Deer, and V. Borisevich for technical assistance. The Jurkat-EBOV, Jurkat-BDBV, and Jurkat-SUDV GP cell lines were a kind gift from C. Davis and R. Ahmed. This work was supported by US NIH grants U19 AI109711 to J.E.C. and A.B., U19 AI142785 to J.E.C. and T.G., R01 AI067927 to E.O.S., and U19 AI109762 to E.O.S. and A.B.W.); the U.S. Department of Health and Human Services (HHS) contract HHSN272201400058C to J.E.C. and B.J.D.; Defense Threat Reduction Agency (DTRA) grant HDTRA1-13-1-0034 to J.E.C. and A.B.; Defense Advanced Reseach Projects Agency (DARPA) grant W31P4Q-14-1-0010 to J.E.C.; Fogarty International Center of the NIH under award number D43TW009343; and the University of California Global Health Institute (UCGHI) to M.S.B.; and funding from the Bill and Melinda Gates Foundation to. J.E.C. by subcontract from Atreca, Inc. E.O.S. is an Investigator in the Pathogenesis of Infectious Disease of the Burroughs Welcome Fund. The project was supported by NCRR grant UL1 RR024975-01, which is now at the National Center for Advancing Translational Sciences, Grant 2 UL1 TR000445-06. The content is solely the responsibility of the authors and does not necessarily represent the official views of the NIH. Work in BSL-4 and ABSL-4 was supported by NIH grant 5UC7AI094660-07 and by the Animal Resource Center of the Galveston National Laboratory.

AUTHOR CONTRIBUTIONS

P.G., C.D.M. B.J.D., R.C., G.K.L., G.A., A. Bukreyev, A.B.W., E.O.S., T.W.G., and J.E.C. planned the studies. P.G., C.D.M., P.A.I., K.H., N.K., R.W.C., C.E.M., J.C.M., P.X.A., S.H., B.M.G., A.L.B., E.D., H.L.T., T.A., R.F., C.O., R.N., R.G.B., S.L., M.E.V., and T.W.G. conducted experiments. A.O., M.I. and B.O. assisted with human sample acquisition. P.G., C.D.M., J.C.M., B.M.G., G.K.L., E.O.S., A.B.W., A. Bukreyev, and J.E.C. interpreted the studies. P.G. and J.E.C. wrote the first draft of the paper. E.O.S., B.J.D, A.B, T.W.G., and J.E.C. obtained funding. All authors reviewed, edited, and approved the paper.

DECLARATION OF INTERESTS

A.L.B., E.D., and B.J.D. are employees of Integral Molecular. B.J.D. is a shareholder of Integral Molecular. J.E.C. has served as a consultant for Sanofi and is on the Scientific Advisory Boards of CompuVax and Meissa Vaccines, is a recipient of previous unrelated research grants from Moderna and Sanofi, and is founder of IDBiologics. Vanderbilt University has applied for a patent that is related to this work. All other authors declare no competing interests.

Received: June 25, 2019
Revised: November 14, 2019
Accepted: January 8, 2020
Published: February 4, 2020

REFERENCES

Adams, P.D., Afonine, P.V., Bunkyczi, G., Chen, V.B., Davis, I.W., Echols, N., Headd, J.J., Hung, L.W., Kapral, G.J., Grosse-Kunstleve, R.W., et al. (2010). PHENIX: a comprehensive Python-based system for macromolecular structure solution. Acta Crystallogr. D Biol. Crystallogr. *66*, 213–221.

Agirre, J., Iglesias-Fernőndez, J., Rovira, C., Davies, G.J., Wilson, K.S., and Cowtan, K.D. (2015). Privateer: software for the conformational validation of carbohydrate structures. Nat. Struct. Mol. Biol. *22*, 833–834.

Barad, B.A., Echols, N., Wang, R.Y., Cheng, Y., DiMaio, F., Adams, P.D., and Fraser, J.S. (2015). EMRinger: side chain-directed model and map validation for 3D cryo-electron microscopy. Nat. Methods *12*, 943–946.

Battye, T.G., Kontogiannis, L., Johnson, O., Powell, H.R., and Leslie, A.G. (2011). iMOSFLM: a new graphical interface for diffraction-image processing with MOSFLM. Acta Crystallogr. D Biol. Crystallogr. *67*, 271–281.

Bendell, C.J., Liu, S., Aumentado-Armstrong, T., Istrate, B., Cernek, P.T., Khan, S., Picioreanu, S., Zhao, M., and Murgita, R.A. (2014). Transient protein-protein interface prediction: datasets, features, algorithms, and the RAD-T predictor. BMC Bioinformatics *15*, 82.

Bennett, R.S., Huzella, L.M., Jahrling, P.B., Bollinger, L., Olinger, G.G., Jr., and Hensley, L.E. (2017). Nonhuman primate models of Ebola virus disease. Curr. Top. Microbiol. Immunol. *411*, 171–193.

Biasini, M., Bienert, S., Waterhouse, A., Arnold, K., Studer, G., Schmidt, T., Kiefer, F., Gallo Cassarino, T., Bertoni, M., Bordoli, L., and Schwede, T. (2014). SWISS-MODEL: modelling protein tertiary and quaternary structure using evolutionary information. Nucleic Acids Res. *42*, W252–W258.

Bornholdt, Z.A., Herbert, A.S., Mire, C.E., He, S., Cross, R.W., Wec, A.Z., Abelson, D.M., Geisbert, J.B., James, R.M., Rahim, M.N., et al. (2019). A two-antibody pan-ebolavirus cocktail confers broad therapeutic protection in ferrets and nonhuman primates. Cell Host Microbe *25*, 49–58.e5.

Bornholdt, Z.A., Turner, H.L., Murin, C.D., Li, W., Sok, D., Souders, C.A., Piper, A.E., Goff, A., Shamblin, J.D., Wollen, S.E., et al. (2016). Isolation of potent neutralizing antibodies from a survivor of the 2014 Ebola virus outbreak. Science *351*, 1078–1083.

Bray, M., Davis, K., Geisbert, T., Schmaljohn, C., and Huggins, J. (1998). A mouse model for evaluation of prophylaxis and therapy of Ebola hemorrhagic fever. J. Infect. Dis. *178*, 651–661.

Bunkyczi, G., and Read, R.J. (2011). Improvement of molecular-replacement models with Sculptor. Acta Crystallogr. D Biol. Crystallogr. *67*, 303–312.

Carlsen, T.H.R., Pedersen, J., Prentoe, J.C., Giang, E., Keck, Z.Y., Mikkelsen, L.S., Law, M., Foung, S.K.H., and Bukh, J. (2014). Breadth of neutralization and synergy of clinically relevant human monoclonal antibodies against HCV genotypes 1a, 1b, 2a, 2b, 2c, and 3a. Hepatology *60*, 1551–1562.

CDC (2019). Ebola in Democratic Republic of the Congo. https://wwwnc.cdc.gov/travel/notices/alert/ebola-democratic-republic-of-the-congo.

Chou, T.C. (2010). Drug combination studies and their synergy quantification using the Chou-Talalay method. Cancer Res. *70*, 440–446.

Coltart, C.E., Lindsey, B., Ghinai, I., Johnson, A.M., and Heymann, D.L. (2017). The Ebola outbreak, 2013-2016: old lessons for new epidemics. Philos. Trans. R. Soc. Lond. B Biol. Sci. *372*, 1–24.

Corti, D., Misasi, J., Mulangu, S., Stanley, D.A., Kanekiyo, M., Wollen, S., Ploquin, A., Doria-Rose, N.A., Staupe, R.P., Bailey, M., et al. (2016a). Protective monotherapy against lethal Ebola virus infection by a potently neutralizing antibody. Science *351*, 1339–1342.

Corti, D., Passini, N., Lanzavecchia, A., and Zambon, M. (2016b). Rapid generation of a human monoclonal antibody to combat Middle East respiratory syndrome. J. Infect. Public Health *9*, 231–235.

Crowe, J.E., Jr. (2017). Principles of broad and potent antiviral human antibodies: Insights for Vaccine Design. Cell Host Microbe *22*, 193–206.

Davidson, E., and Doranz, B.J. (2014). A high-throughput shotgun mutagenesis approach to mapping B-cell antibody epitopes. Immunology *143*, 13–20.

Davidson, E., Bryan, C., Fong, R.H., Barnes, T., Pfaff, J.M., Mabila, M., Rucker, J.B., and Doranz, B.J. (2015). Mechanism of binding to Ebola virus glycoprotein by the ZMapp, ZMAb, and MB-003 cocktail antibodies. J. Virol. *89*, 10982–10992.

Davis, C.W., Jackson, K.J.L., McElroy, A.K., Halfmann, P., Huang, J., Chennareddy, C., Piper, A.E., Leung, Y., Albarino, C.G., Crozier, I., et al. (2019). Longitudinal analysis of the human B cell response to Ebola virus infection. Cell *177*, 1566–1582.

DiMaio, F., Song, Y., Li, X., Brunner, M.J., Xu, C., Conticello, V., Egelman, E., Marlovits, T., Cheng, Y., and Baker, D. (2015). Atomic-accuracy models from 4.5-Å cryo-electron microscopy data with density-guided iterative local refinement. Nat. Methods *12*, 361–365.

Domi, A., Feldmann, F., Basu, R., McCurley, N., Shifflett, K., Emanuel, J., Hellerstein, M.S., Guirakhoo, F., Orlandi, C., Flinko, R., et al. (2018). A single dose of modified Vaccinia Ankara expressing Ebola virus like particles protects nonhuman primates from lethal Ebola virus challenge. Sci. Rep. *8*, 864.

Doria-Rose, N.A., Louder, M.K., Yang, Z., O'Dell, S., Nason, M., Schmidt, S.D., McKee, K., Seaman, M.S., Bailer, R.T., and Mascola, J.R. (2012). HIV-1 neutralization coverage is improved by combining monoclonal antibodies that target independent epitopes. J. Virol. *86*, 3393–3397.

Emsley, P., Lohkamp, B., Scott, W.G., and Cowtan, K. (2010). Features and development of Coot. Acta Crystallogr. D Biol. Crystallogr. *66*, 486–501.

Evans, P.R., and Murshudov, G.N. (2013). How good are my data and what is the resolution? Acta Crystallogr. D Biol. Crystallogr. *69*, 1204–1214.

Fibriansah, G., Ibarra, K.D., Ng, T.S., Smith, S.A., Tan, J.L., Lim, X.N., Ooi, J.S., Kostyuchenko, V.A., Wang, J., de Silva, A.M., et al. (2015). DENGUE VIRUS. Cryo-EM structure of an antibody that neutralizes dengue virus type 2 by locking E protein dimers. Science *349*, 88–91.

Flyak, A.I., Ilinykh, P.A., Murin, C.D., Garron, T., Shen, X., Fusco, M.L., Hashiguchi, T., Bornholdt, Z.A., Slaughter, J.C., Sapparapu, G., et al. (2015). Mechanism of human antibody-mediated neutralization of Marburg virus. Cell *160*, 893–903.

Geisbert, T.W., Mire, C.E., Geisbert, J.B., Chan, Y.P., Agans, K.N., Feldmann, F., Fenton, K.A., Zhu, Z., Dimitrov, D.S., Scott, D.P., et al. (2014). Therapeutic treatment of Nipah virus infection in nonhuman primates with a neutralizing human monoclonal antibody. Sci. Transl. Med. *6*, 242ra82.

Geisbert, T.W., Strong, J.E., and Feldmann, H. (2015). Considerations in the use of nonhuman primate models of Ebola virus and Marburg virus infection. J. Infect. Dis. *212*, S91–S97.

Gilchuk, I., Gilchuk, P., Sapparapu, G., Lampley, R., Singh, V., Kose, N., Blum, D.L., Hughes, L.J., Satheshkumar, P.S., Townsend, M.B., et al. (2016). Cross-neutralizing and protective human antibody specificities to poxvirus infections. Cell *167*, 684–694.

Gilchuk, P., Kuzmina, N., Ilinykh, P.A., Huang, K., Gunn, B.M., Bryan, A., Davidson, E., Doranz, B.J., Turner, H.L., Fusco, M.L., et al. (2018). Multifunctional pan-ebolavirus antibody recognizes a site of broad vulnerability on the ebolavirus glycoprotein. Immunity *49*, 363–374.

Giudicelli, V., and Lefranc, M.P. (2011). IMGT/junctionanalysis: IMGT standardized analysis of the V-J and V-D-J junctions of the rearranged immunoglobulins (IG) and T cell receptors (TR). Cold Spring Harb. Protoc. *2011*, 716–725.

Gunn, B.M., Yu, W.H., Karim, M.M., Brannan, J.M., Herbert, A.S., Wec, A.Z., Halfmann, P.J., Fusco, M.L., Schendel, S.L., Gangavarapu, K., et al. (2018). A role for Fc function in therapeutic monoclonal antibody-mediated protection against Ebola virus. Cell Host Microbe *24*, 221–233.

Howell, K.A., Brannan, J.M., Bryan, C., McNeal, A., Davidson, E., Turner, H.L., Vu, H., Shulenin, S., He, S., Kuehne, A., et al. (2017). Cooperativity enables non-neutralizing antibodies to neutralize ebolavirus. Cell Rep. *19*, 413–424.

Ilinykh, P.A., Shen, X., Flyak, A.I., Kuzmina, N., Ksiazek, T.G., Crowe, J.E., Jr., and Bukreyev, A. (2016). Chimeric filoviruses for identification and characterization of monoclonal antibodies. J. Virol. *90*, 3890–3901.

Keeffe, J.R., Van Rompay, K.K.A., Olsen, P.C., Wang, Q., Gazumyan, A., Azzopardi, S.A., Schaefer-Babajew, D., Lee, Y.E., Stuart, J.B., Singapuri, A., et al. (2018). A Combination of two human monoclonal antibodies prevents Zika virus escape mutations in non-human primates. Cell. Rep. *25*, 1385–1394.

King, L.B., Milligan, J.C., West, B.R., Schendel, S.L., and Ollmann Saphire, E. (2019). Achieving cross-reactivity with pan-ebolavirus antibodies. Curr. Opin. Virol. *34*, 140–148.

Kuhn, J.H. (2017). Guide to the Correct Use of Filoviral Nomenclature. In Marburg- and Ebolaviruses. Curr. Top. Microbiol, *Volume 411*, E. Mьhlberger, L. Hensley, and J. Towner, eds. (Cham: Springer), pp. 447–460.

Kuzmina, N.A., Younan, P., Gilchuk, P., Santos, R.I., Flyak, A.I., Ilinykh, P.A., Huang, K., Lubaki, N.M., Ramanathan, P., Crowe, J.E., Jr., et al. (2018). Antibody-dependent enhancement of Ebola virus infection by human antibodies isolated from survivors. Cell. Rep. *24*, 1802–1815.

Lander, G.C., Stagg, S.M., Voss, N.R., Cheng, A., Fellmann, D., Pulokas, J., Yoshioka, C., Irving, C., Mulder, A., Lau, P.W., et al. (2009). Appion: an

integrated, database-driven pipeline to facilitate EM image processing. J. Struct. Biol. *166*, 95–102.

Laursen, N.S., and Wilson, I.A. (2013). Broadly neutralizing antibodies against influenza viruses. Antiviral Res. *98*, 476–483.

Lee, J.E., and Saphire, E.O. (2009). Ebolavirus glycoprotein structure and mechanism of entry. Future Virol. *4*, 621–635.

Lu, L.L., Suscovich, T.J., Fortune, S.M., and Alter, G. (2018). Beyond binding: antibody effector functions in infectious diseases. Nat. Rev. Immunol. *18*, 46–61.

Lütteke, T., and von der Lieth, C.W. (2004). pdb-care (PDB carbohydrate residue check): a program to support annotation of complex carbohydrate structures in PDB files. BMC Bioinformatics *5*, 69.

Mascola, J.R., Louder, M.K., VanCott, T.C., Sapan, C.V., Lambert, J.S., Muenz, L.R., Bunow, B., Birx, D.L., and Robb, M.L. (1997). Potent and synergistic neutralization of human immunodeficiency virus (HIV) type 1 primary isolates by hyperimmune anti-HIV immunoglobulin combined with monoclonal antibodies 2F5 and 2G12. J. Virol. *71*, 7198–7206.

McLean, G.R., Nakouzi, A., Casadevall, A., and Green, N.S. (2000). Human and murine immunoglobulin expression vector cassettes. Mol. Immunol. *37*, 837–845.

Mohan, G.S., Li, W., Ye, L., Compans, R.W., and Yang, C. (2012). Antigenic subversion: a novel mechanism of host immune evasion by Ebola virus. PLoS Pathog. *8*, e1003065.

Murin, C.D., Bruhn, J.F., Bornholdt, Z.A., Copps, J., Stanfield, R., and Ward, A.B. (2018). Structural basis of pan-ebolavirus neutralization by an antibody targeting the glycoprotein fusion loop. Cell. Rep. *24*, 2723–2732.

Nature News (2019). Two Ebola drugs show promise amid ongoing outbreak, (accessed 26 September 2019) https://www.nature.com/articles/d41586-019-02442-6.

NIH (2019). Investigational Therapeutics for the Treatment of People With Ebola Virus Disease, (accessed 11 June 2019) https://clinicaltrials.gov/ct2/show/NCT03719586?cond=ebola&rank=7.

Orlandi, C., Flinko, R., and Lewis, G.K. (2016). A new cell line for high throughput HIV-specific antibody-dependent cellular cytotoxicity (ADCC) and cell-to-cell virus transmission studies. J. Immunol. Methods *433*, 51–58.

Park, D.J., Dudas, G., Wohl, S., Goba, A., Whitmer, S.L., Andersen, K.G., Sealfon, R.S., Ladner, J.T., Kugelman, J.R., Matranga, C.B., et al. (2015). Ebola virus epidemiology, transmission, and evolution during seven months in Sierra Leone. Cell *161*, 1516–1526.

Pascal, K.E., Dudgeon, D., Trefry, J.C., Anantpadma, M., Sakurai, Y., Murin, C.D., Turner, H.L., Fairhurst, J., Torres, M., Rafique, A., et al. (2018). Development of clinical-stage human monoclonal antibodies that treat advanced Ebola virus disease in nonhuman primates. J. Infect. Dis. *218*, S612–S626.

Pettersen, E.F., Goddard, T.D., Huang, C.C., Couch, G.S., Greenblatt, D.M., Meng, E.C., and Ferrin, T.E. (2004). UCSF Chimera–a visualization system for exploratory research and analysis. J. Comput. Chem. *25*, 1605–1612.

Potter, C.S., Chu, H., Frey, B., Green, C., Kisseberth, N., Madden, T.J., Miller, K.L., Nahrstedt, K., Pulokas, J., Reilein, A., et al. (1999). Leginon: a system for fully automated acquisition of 1000 electron micrographs a day. Ultramicroscopy *77*, 153–161.

Punjani, A., Rubinstein, J.L., Fleet, D.J., and Brubaker, M.A. (2017). cryoSPARC: algorithms for rapid unsupervised cryo-EM structure determination. Nat. Methods *14*, 290–296.

Raymond, J., Bradfute, S., and Bray, M. (2011). Filovirus infection of STAT-1 knockout mice. J. Infect. Dis. *204*, S986–S990.

Robinson, J.E., Hastie, K.M., Cross, R.W., Yenni, R.E., Elliott, D.H., Rouelle, J.A., Kannadka, C.B., Smira, A.A., Garry, C.E., Bradley, B.T., et al. (2016). Most neutralizing human monoclonal antibodies target novel epitopes requiring both Lassa virus glycoprotein subunits. Nat. Commun. *7*, 11544.

Sanchez, A., and Rollin, P.E. (2005). Complete genome sequence of an Ebola virus (Sudan species) responsible for a 2000 outbreak of human disease in Uganda. Virus Res. *113*, 16–25.

Sapparapu, G., Fernandez, E., Kose, N., Bin Cao, Fox, J.M., Bombardi, R.G., Zhao, H., Nelson, C.A., Bryan, A.L., Barnes, T., et al. (2016). Neutralizing human antibodies prevent Zika virus replication and fetal disease in mice. Nature *540*, 443–447.

Scheres, S.H. (2012). RELION: implementation of a Bayesian approach to cryo-EM structure determination. J. Struct. Biol. *180*, 519–530.

Sok, D., and Burton, D.R. (2018). Recent progress in broadly neutralizing antibodies to HIV. Nat. Immunol. *19*, 1179–1188.

Stettler, K., Beltramello, M., Espinosa, D.A., Graham, V., Cassotta, A., Bianchi, S., Vanzetta, F., Minola, A., Jaconi, S., Mele, F., et al. (2016). Specificity, cross-reactivity, and function of antibodies elicited by Zika virus infection. Science *353*, 823–826.

Towner, J.S., Paragas, J., Dover, J.E., Gupta, M., Goldsmith, C.S., Huggins, J.W., and Nichol, S.T. (2005). Generation of eGFP expressing recombinant Zaire ebolavirus for analysis of early pathogenesis events and high-throughput antiviral drug screening. Virology *332*, 20–27.

Turchaninova, M.A., Davydov, A., Britanova, O.V., Shugay, M., Bikos, V., Egorov, E.S., Kirgizova, V.I., Merzlyak, E.M., Staroverov, D.B., Bolotin, D.A., et al. (2016). High-quality full-length immunoglobulin profiling with unique molecular barcoding. Nat. Protoc. *11*, 1599–1616.

Urbanowicz, R.A., McClure, C.P., Sakuntabhai, A., Sall, A.A., Kobinger, G., Mьller, M.A., Holmes, E.C., Rey, F.A., Simon-Loriere, E., and Ball, J.K. (2016). Human adaptation of Ebola virus during the West African outbreak. Cell *167*, 1079–1087.e5.

Voss, N.R., Yoshioka, C.K., Radermacher, M., Potter, C.S., and Carragher, B. (2009). DoG Picker and TiltPicker: software tools to facilitate particle selection in single particle electron microscopy. J. Struct. Biol. *166*, 205–213.

Walker, L.M., and Burton, D.R. (2018). Passive immunotherapy of viral infections: 'super-antibodies' enter the fray. Nat. Rev. Immunol. *18*, 297–308.

Wang, Q., Yang, H., Liu, X., Dai, L., Ma, T., Qi, J., Wong, G., Peng, R., Liu, S., Li, J., et al. (2016b). Molecular determinants of human neutralizing antibodies isolated from a patient infected with Zika virus. Sci. Transl. Med. *8*, 369ra179.

Wec, A.Z., Bornholdt, Z.A., He, S., Herbert, A.S., Goodwin, E., Wirchnianski, A.S., Gunn, B.M., Zhang, Z., Zhu, W., Liu, G., et al. (2019). Development of a human antibody cocktail that deploys multiple functions to confer pan-ebolavirus protection. Cell Host Microbe *25*, 39–48.

Wec, A.Z., Herbert, A.S., Murin, C.D., Nyakatura, E.K., Abelson, D.M., Fels, J.M., He, S., James, R.M., de La Vega, M.A., Zhu, W., et al. (2017). Antibodies from a human survivor define sites of vulnerability for broad protection against ebolaviruses. Cell *169*, 878–890.

West, B.R., Moyer, C.L., King, L.B., Fusco, M.L., Milligan, J.C., Hui, S., and Saphire, E.O. (2018). Structural basis of pan-ebolavirus neutralization by a human antibody against a conserved, yet cryptic epitope. MBio. https://doi.org/10.1128/mBio.01674-18.

West, B.R., Wec, A.Z., Moyer, C.L., Fusco, M.L., Ilinykh, P.A., Huang, K., Wirchnianski, A.S., James, R.M., Herbert, A.S., Hui, S., et al. (2019). Structural basis of broad Ebola virus neutralization by a human survivor antibody. Nat. Struct. Mol. Biol. *26*, 204–212.

Williams, C.J., Headd, J.J., Moriarty, N.W., Prisant, M.G., Videau, L.L., Deis, L.N., Verma, V., Keedy, D.A., Hintze, B.J., Chen, V.B., et al. (2018). MolProbity: More and better reference data for improved all-atom structure validation. Protein Sci. *27*, 293–315.

Yu, X., McGraw, P.A., House, F.S., and Crowe, J.E., Jr. (2008). An optimized electrofusion-based protocol for generating virus-specific human monoclonal antibodies. J. Immunol. Methods *336*, 142–151.

Zhang, K. (2016). Gctf: Real-time CTF determination and correction. J. Struct. Biol. *193*, 1–12.

Zhao, Z., and Singer, A. (2014). Rotationally invariant image representation for viewing direction classification in cryo-EM. J. Struct. Biol. *186*, 153–166.

Zhao, Y., Ren, J., Harlos, K., Jones, D.M., Zeltina, A., Bowden, T.A., Padilla-Parra, S., Fry, E.E., and Stuart, D.I. (2016). Toremifene interacts with and destabilizes the Ebola virus glycoprotein. Nature *535*, 169–172.

Zheng, S.Q., Palovcak, E., Armache, J.P., Verba, K.A., Cheng, Y., and Agard, D.A. (2017). MotionCor2: anisotropic correction of beam-induced motion for improved cryo-electron microscopy. Nat. Methods *14*, 331–332.

Zivanov, J., Nakane, T., Forsberg, B.O., Kimanius, D., Hagen, W.J., Lindahl, E., and Scheres, S.H. (2018). New tools for automated high-resolution cryo-EM structure determination in RELION-3. eLife *7*, e42166.

STAR★METHODS

KEY RESOURCES TABLE

REAGENT or RESOURCE	SOURCE	IDENTIFIER
Antibodies		
rEBOV-520 IgG1 (recombinant CHO-produced)	Gilchuk et al., 2018	N/A
rEBOV-520 IgG1-LALA (recombinant CHO-produced)	Gilchuk et al., 2018	N/A
rEBOV-548 IgG1 (recombinant CHO-produced)	This paper	N/A
c13C6 (recombinant CHO-produced IgG1)	This study	N/A
c13C6	IBT Bioservices	N/A
EBOV-437(hybridoma-produced IgG1)	Gilchuk et al., 2018	N/A
EBOV-442 (hybridoma-produced IgG1)	Gilchuk et al., 2018	N/A
EBOV-515 (hybridoma-produced IgG1)	Gilchuk et al., 2018	N/A
2D22 (hybridoma-produced IgG1)	Fibriansah et al., 2015	N/A
Goat anti-human IgG-HRP	Southern Biotech	Cat#2040-05; RRID: AB_2795644
Goat anti-human IgG-PE	Southern Biotech	Cat#2040-09; RRID: AB_2795648
Mouse Anti-Human IgG_1 Hinge-AP	Southern Biotech	Cat#9052-04; RRID: AB_2687996
Mouse Anti-Human IgG_2 Fc-AP	Southern Biotech	Cat#9070-04; RRID: AB_2687997
Mouse Anti-Human IgG3 Hinge-AP	Southern Biotech	Cat#9210-04; RRID: AB_2687998
Mouse Anti-Human IgG4 Fc-AP	Southern Biotech	Cat#9200-04; RRID: AB_2687999
rEBOV-520 Fab	This paper	N/A
rEBOV-548 Fab	This paper	N/A
rEBOV-520 IgG1-LALA/Alexa Fluor 647	This paper	N/A
rEBOV-548 IgG1/Alexa Fluor 647	This paper	N/A
Pacific Blue anti-human CD66b Antibody (clone G10F5)	BioLegend	Cat#305112; RRID: AB_2563294
Alexa Fluor 700 Mouse Anti-Human CD3 (clone UCHT1)	BD Biosciences	Cat#557943; RRID: AB_396952
APC-Cy7 Mouse Anti-Human CD14 (clone MφP9)	BD Biosciences	Cat#561709; RRID: AB_10893806
PE-Cy5 Mouse Anti-Human CD107a (clone H4A3)	BD Biosciences	Cat#555802; RRID: AB_396136
PE-Cy7 Mouse Anti-Human CD56 (clone B159)	BD Biosciences	Cat#557747; RRID: AB_396853
APC-Cy7 Mouse Anti-Human CD16 (clone 3G8)	BD Biosciences	Cat#557758; RRID: AB_396864
APC Mouse Anti-Human IFN-γ (clone B27)	BD Biosciences	Cat#554702; RRID: AB_398580
PE Mouse Anti-Human MIP-1β (clone D21-1351)	BD Biosciences	Cat#550078; RRID: AB_393549
Mouse anti-Human IgG (CH2 domain) Secondary Antibody	Thermo Fisher Scientific	Cat#MA5-16929; RRID: AB_2538406
Bacterial and Virus Strains		
Mouse-adapted EBOV /Mayinga (EBOV/M.mus-tc/COD/76/Yambuku-Mayinga, GenBank: AF499101)	Bray et al., 1998	N/A
EBOV-eGFP/Mayinga	Towner et al., 2005	N/A
SUDV strain Gulu (GenBank: AY729654)	Sanchez and Rollin, 2005	N/A
Chimeric EBOV/BDBV-GP (GenBank: KU174137)	Ilinykh et al., 2016	N/A
Chimeric EBOV/SUDV-GP (GenBank: KU174142)	Ilinykh et al., 2016	N/A
L273P EBOV-eGFP, mAb rEBOV-548 escape mutant	This paper	N/A
Biological Samples		
PBMCs from EVD survivor (2013-2016 EVD epidemic in Nigeria)	This paper	Donor ID #963
Chemicals, Peptides, and Recombinant Proteins		
EBOV GP ΔTM (aa 1-636; Makona)	This paper	N/A
BDBV GP ΔTM (aa 1-643; 200706291 Uganda)	This paper	N/A

(*Continued on next page*)

Continued

REAGENT or RESOURCE	SOURCE	IDENTIFIER
SUDV GP ΔTM (aa 1-637; Gulu)	This paper	N/A
MARV GP ΔTM (aa 1-648; Angola 2005)	This paper	N/A
EBOV GPΔMuc	This paper	N/A
EBOV GP ΔTM	IBT Bioservices	Cat#0501-016
Thermolysin	Promega	Cat#9PIV400
Immobilized papain	ThermoFisher	Cat#20341
Brefeldin A	Sigma Aldrich	Cat#B7651
GolgiStop	BD Biosciences	Cat#554724
Step-Tactin resin	QIAGEN	Cat#30002
Alexa Fluor 647 NHS ester	ThermoFisher	Cat#A37573
FluoSpheres NeutrAvidin®-Labeled Microspheres	ThermoFisher	Cat#F-8776
EZ-Link™ Sulfo-NHS-LC-LC-Biotin	ThermoFisher	Cat#21338
1-Step Ultra TMB-ELISA	ThermoFisher	Cat#34029
Freestyle 293 expression medium	ThermoFisher	Cat#12338002
ExpiCHO Expression Medium	ThermoFisher	Cat#A2910001
Fetal Bovine Serum, ultra-low IgG	ThermoFisher	Cat#16250078
ClonaCell-HY Medium E	Stem Cell Technologies	Cat#03805
ClonaCell-HY Medium A	Stem Cell Technologies	Cat#03801
Critical Commercial Assays		
RosetteSep Human NK Cell Enrichment Cocktail	Stem Cell Technologies	Cat#15025
Diagnostic Profile Reagent Rotor Package	Abaxis	Cat#500-0038
Deposited Data		
rEBOV-520/rEBOV-548 Fab complex with EBOV GP ΔTM Mayinga (negative stain EM)	This paper	EMD-20293
rEBOV-520/rEBOV-548 Fab complex with EBOV GP ΔMucΔTM Makona (cryo-EM)	This paper	EMD-20301; PDB: 6PCI
rEBOV-548 Fab complex with EBOV GP ΔMucΔTM Makona (cryo-EM)	This paper	EMD-20947; PDB: 6UYE
EBOV GP_{CL} + EBOV-520 Fab crystal structure	This paper	PDB: 6OZ9
Experimental Models: Cell Lines		
Human: Jurkat, clone E6-1	ATCC	ATCC: TIB-152; RRID: CVCL_0367
Human: Jurkat-EBOV GP (Makona)	Davis et al., 2019; Gilchuk et al., 2018	N/A
Human: Jurkat-SUDV GP (Gulu)	C. Davis and R. Ahmed	N/A
Human: Jurkat-BDBV GP (Uganda)	C. Davis and R. Ahmed	N/A
Human: Jurkat-MARV GP (Angola)	C. Davis and R. Ahmed	N/A
Mouse: NIH 3T3-hCD40-hIL21-hBAFF	D. Bhattacharya	N/A
Mouse-human trioma MFP-2 (B6B11)	ATCC	ATCC: HB-12481; RRID: CVCL_9V32
Hamster: ExpiCHO-S	ThermoFisher Scientific	Cat#A29127; RRID: CVCL_5J31
Human: FreeStyle 293-F	ThermoFisher Scientific	Cat#R79007; RRID: CVCL_D603
Human: THP-1 monocytes	ATCC	ATCC: TIB-202; RRID: CVCL_0006
Human: EBOV GPkik-293FS EGFP CCR5-SNAP	J. Lewis	N/A
Monkey: Vero-E6	ATCC	ATCC: CRL-1586; RRID: CVCL_0574
Drosophila: Schneider 2	ThermoFisher Scientific	Cat#R69007; RRID: CVCL_Z232
EBOV-437 hybridoma clone	Gilchuk et al., 2018	N/A
EBOV-442 hybridoma clone	Gilchuk et al., 2018	N/A
EBOV-542 hybridoma clone	This study	N/A
EBOV-548 hybridoma clone	This study	N/A

(*Continued on next page*)

Continued

REAGENT or RESOURCE	SOURCE	IDENTIFIER
Experimental Models: Organisms/Strains		
Mouse: BALB/cJ	The Jackson Laboratory	Cat#JAX:000651; RRID: IMSR_JAX:000651
Mouse: 129S6/SvEv-Stat1^{tm1Rds} (STAT1 KO)	Taconic Biosciences	Cat#TAC:2045; RRID: IMSR_TAC:2045
NHP: Macaca mulatta, Chinese origin	PrimGen	N/A
Recombinant DNA		
Plasmid: EBOV GP ΔTM (aa 1-636; Makona)	Gilchuk et al., 2018	N/A
Plasmid: BDBV GP ΔTM (aa 1-643; 200706291 Uganda)	Gilchuk et al., 2018	N/A
Plasmid: SUDV GP ΔTM (aa 1-637; Gulu)	Gilchuk et al., 2018	N/A
Plasmid: MARV GP ΔTM (aa 1-648; Angola 2005)	This paper	N/A
Plasmid: EBOV-520 rIgG1 heavy chain	Gilchuk et al., 2018	N/A
Plasmid: EBOV-520 light chain	Gilchuk et al., 2018	N/A
Plasmid: EBOV-520 rIgG1-LALA heavy chain	Gilchuk et al., 2018	N/A
Plasmid: EBOV-520 Fab heavy chain	Gilchuk et al., 2018	N/A
Plasmid: EBOV-548 rIgG1 heavy chain	This paper	N/A
Plasmid: EBOV-548 light chain	This paper	N/A
Plasmid: EBOV-548 Fab heavy chain	This paper	N/A
Software and Algorithms		
GraphPad Prism 7.2	GraphPad Software, Inc.	GraphPad Prism; RRID: SCR_002798
CompuSyn	Chou, 2010	CompuSyn
ForeCyt Standard 6.2 (R1)	Intellicyt	ForeCyt
RTCA version 2.1.0	Acea Biosciences, Inc	RTCA Software; RRID: SCR_014821
DynamX 3.0	Waters Corp	DynamX
FlowJo version 10	Tree Star Inc.	FlowJo; RRID: SCR_008520
ImMunoGeneTics database	Giudicelli and Lefranc, 2011	IMGT - the international ImMunoGeneTics information system; RRID: SCR_012780
DoG picker	Voss et al., 2009	DoG picker
Appion	Lander et al., 2009	Appion Package; RRID: SCR_016734
MotionCorr2	Zheng et al., 2017	MotionCorr2
GCTF	Zhang, 2016	GCTF; RRID: SCR_016500
Cryosparc2	Punjani et al., 2017	Cryosparc2
Leginon	Potter et al., 1999	Leginon; RRID: SCR_016731
RELION 3.0	Zivanov et al., 2018	RELION; RRID: SCR_016274
UCSF Chimera	Pettersen et al., 2004	UCSF Chimera; RRID: SCR_004097
Phenix	Adams et al., 2010	Phenix; RRID: SCR_014224
Rosetta	DiMaio et al., 2015	Rosetta; RRID: SCR_015701
MolProbity	Williams et al., 2018	MolProbity; RRID: SCR_014226
EMRinger	Barad et al., 2015	EMRinger
Coot	Emsley et al., 2010	Coot; RRID: SCR_014222
PDB-care	Lütteke and von der Lieth, 2004	PDB-care; RRID: SCR_001562
Privateer	Agirre et al., 2015	Privateer
Other		
VetScan VS2 Chemistry Analyzer	Abaxis	N/A
iQue Screener Plus flow cytometer	Intellicyt	N/A
BD LSR2 (3-laser) flow cytometer	BD Biosciences	N/A
ECM 2001 Electro Cell Manipulator	BTX	N/A
ÄKTA pure chromatography system	GE Healthcare Life Sciences	
Tecnai Spirit electron microscope with TemCam F416 4k x 4k CCD	ThermoFisher Scientific	N/A

(*Continued on next page*)

Continued

REAGENT or RESOURCE	SOURCE	IDENTIFIER
Synergy H1 microplate reader	BioTek	N/A
Synergy 2 microplate reader	BioTek	N/A
EL406 washer dispenser	BioTek	N/A
Biostack microplate stacker	BioTek	N/A
StrepTrap HP	GE Healthcare Life Sciences	N/A
HiTrap Protein G High Performance	GE Healthcare Life Sciences	Cat#28-9075-48
HiTrap MabSelect™ SuRe 5 mL column	GE Healthcare Life Sciences	Cat#17-0404-01
Superdex 200 Increase 10/300 GL column	GE Healthcare Life Sciences	Cat#PI-89883
xCELLigence RTCA MP analyzer	Acea Biosciences, Inc	N/A

LEAD CONTACT AND MATERIALS AVAILABILITY

Further information and requests for resources and reagents should be directed to and will be fulfilled by the Lead Contact, James E. Crowe, Jr. (james.crowe@vumc.org). Materials described in this paper are available for distribution under the Uniform Biological Material Transfer Agreement, a master agreement that was developed by the NIH to simplify transfers of biological research materials.

EXPERIMENTAL MODEL AND SUBJECT DETAILS

Human samples

Human PBMCs were obtained from a survivor of the 2014 EVD epidemic in Nigeria. A male human survivor of the 2014 EVD outbreak in Nigeria was age 31 when infected and age 32 when PBMCs were collected. PBMCs were collected after the illness had resolved, following written informed consent. At time of blood collection, plasma samples were tested by qRT-PCR and found to be negative for the presence of viral RNA. The studies were approved by the Institutional Review Board of Vanderbilt University Medical Center.

Cell lines

Vero-E6 (monkey, female origin), THP-1 (human, male origin), and Jurkat (human, male origin) cell lines were obtained from the American Type Culture Collection (ATCC). Vero-E6 cells were cultured in Minimal Essential Medium (MEM) (ThermoFisher Scientific) supplemented with 10% fetal bovine serum (FBS; HyClone) and 1% penicillin-streptomycin at 5% CO_2, 37°C. THP-1 and Jurkat cells were cultured in RPMI 1640 (GIBCO) medium supplemented with 10% heat-inactivated FBS (GIBCO), 1% GlutaMax (GIBCO), 100 units/mL of penicillin, and 100 μg/mL of streptomycin (GIBCO) at 37°C in 5% CO_2. The MFP-2 line is a non-secreting mouse-human trioma cell line (sex information is not available) that was generated by fusing a murine myeloma cell line with a human myeloma cell line, yielding the intermediate heteromyeloma B6B11, followed by fusion with a human lymphocyte. This cell line was cultured as described previously (Yu et al., 2008). A 293F cell line (human, female origin) stably-transfected to express SNAP-tagged EBOV GP was described previously (Domi et al., 2018). ExpiCHO (hamster, female origin) and FreeStyle 293F (human, female origin) cell lines were purchased from ThermoFisher Scientific and cultured according to the manufacturer's protocol. The Jurkat-EBOV GP (variant Makona) (Davis et al., 2019), Jurkat-BDBV GP (strain Uganda), Jurkat-SUDV GP (strain Gulu) cell lines stably transduced to display respective GP on the surface (Davis and Ahmed, unpublished) were a kind gift from Carl Davis (Emory University, Atlanta, GA). An NIH 3T3 engineered fibroblast line (mouse, male origin) constitutively expressing cell-surface human CD154 (CD40 ligand), secreted human B cell activating factor (BAFF) and human IL-21 was kindly provided by Dr. Deepta Bhattacharya (Washington University in St. Louis, MO). All cell lines were tested on a monthly basis for *Mycoplasma* and found to be negative in all cases.

Viruses

The authentic EBOV-eGFP, mouse-adapted EBOV Mayinga (EBOV-MA, GenBank: AF49101) and SUDV strain Gulu were described previously (Bray et al., 1998; Sanchez and Rollin, 2005; Towner et al., 2005). The chimeric infectious EBOV/BDBV-GP and EBOV/SUDV-GP viruses expressing eGFP were obtained by replacing the gene encoding EBOV GP with that of BDBV (GenBank: KU174137) or SUDV (GenBank: KU174142), respectively (Ilinykh et al., 2016).

Mouse models

Seven- to eight-week old female BALB/c mice were obtained from the Jackson Laboratory, and 7- to 8-week-old female 129S6/SvEv-Stat1tm1Rds mice (*Stat1*$^{-/-}$) were obtained from Taconic Biosciences. Mice were housed in microisolator cages and provided food and water *ad libitum*. Challenge studies were conducted under maximum containment in an animal biosafety level 4 (ABSL-4) facility of the Galveston National Laboratory, UTMB. The animal protocols for testing of mAbs in mice were approved by the

Institutional Animal Care and Use Committee of the University of Texas Medical Branch (UTMB) in compliance with the Animal Welfare Act and other applicable federal statutes and regulations relating to animals and experiments involving animals.

NHP model

Four- to six-year old male (n = 3) and female (n = 3) rhesus macaques used in this study were obtained from PrimGen. NHP research adhered to principles stated in the eighth edition of the Guide for the Care and Use of Laboratory Animals. The facility where this research was conducted [University of Texas Medical Branch (UTMB)] is fully accredited by the Association for Assessment and Accreditation of Laboratory Animal Care International and has an approved Office of Laboratory Animal Welfare Assurance (#A3314-01).

METHOD DETAILS

Generation of human B cell hybridomas producing mAbs

PBMCs from a leukopak were isolated with Ficoll-Histopaque by density gradient centrifugation. The cells were cryopreserved in the vapor phase of liquid nitrogen until use. The EBOV GP-reactive memory B cells were labeled with the recombinant EBOV GP protein that was produced in *Drosophila* Schneider 2 (S2) cells as described below and purified by fluorescence activated cell sorting (FACS) as described previously (Bornholdt et al., 2016). This step resulted in ~5,000 sorted EBOV GP-reactive memory B cells. Human B cell hybridomas were generated as described previously (Yu et al., 2008) with some modifications. Briefly, FACS-isolated GP-reactive B cells were bulk-expanded on irradiated NIH 3T3 cells that had been engineered to express human IL-21, CD40L (CD154), and BAFF in medium A (STEMCELL Technologies) supplemented with CpG, a Chk2 inhibitor (Sigma-Aldrich), and cyclosporine A (Sigma-Aldrich). After 8 days cells were bulk-fused with MFP-2 myeloma cells using an established electrofusion technique (Yu et al., 2008), which resulted in generation of ~1,100 individual hybridoma lines. After the fusion reaction, hybridoma lines were cultured in ClonaCell-HY Medium E (STEMCELL Technologies) supplemented with HAT (hypoxanthine-aminopterin-thymidine) Media Supplement (Sigma-Aldrich) in 384-well plates for 18 days before screening of supernatants for antibody production.

Screening strategy to identify partner mAbs for therapeutic cocktail

Our previous work used Jurkat cell surface displayed EBOV GP to assess competition-binding groups of the GP reactive mAbs that isolated from human survivor of EVD outbreak in the DRC (Gilchuk et al., 2018). This study revealed that binding of two broadly-reactive glycan cap specific mAbs increases binding of broadly-neutralizing and highly protective base-specific mAbs EBOV-515 and EBOV-520 (Gilchuk et al., 2018). Here, for the development of cooperative mAb cocktail, we performed a comprehensive screening from ~1,800 individual GP-reactive B cell line supernatants (~1,100 from this study and ~750 from previous study with the DRC outbreak survivor) to identify a suitable partner mAb for these potent base-specific mAb. The criteria for down-selection of the partner mAb candidates included (a) high neutralizing activity against live pathogenic virus (neutralizing at least EBOV); (b) broad reactivity to EBOV, BDBV, and SUDV GP; (c) synergistic activity that was defined as the ability of mAb to enhance binding of EBOV-515 and EBOV-520 (at least 2-fold enhancement) when compared to binding of the base-specific mAb alone; and (d) efficacy of monotherapy in mice to protect against live EBOV challenge. Supernatants from each well of the 384-well culture plates with expanded hybridoma lines first were assessed for neutralizing activity against live EBOV using one 1:5 supernatant dilution in 96-well plate format as detailed below in the **Neutralization assays** section. Next, hybridoma lines that fully neutralized EBOV at the supernatant dilution tested were assessed by ELISA for reactivity against recombinant EBOV, BDBV, and SUDV GP. The broadly-reactive clones identified were tested for neutralizing activity against live BDBV and SUDV. Hybridoma cell lines producing cross-reactive and neutralizing mAbs (mAbs that reacted to all three GPs and neutralized at least EBOV and BDBV) were cloned biologically by single-cell fluorescence-activated cell sorting. Hybridomas were expanded in Medium E (STEMCELL Technologies) until 50% confluent in 75-cm^2 flasks (Corning). Purified mAbs were tested using a competition-binding assay with intact Jurkat-EBOV GP (A) or thermolysin cleaved Jurkat-EBOV GP_{CL} to identify major antigenic sites.

Identified mAbs that (a) competed with the reference glycan cap specific mAbs c13C16 (Davidson et al., 2015) or BDBV289 (Flyak et al., 2916) on intact GP, and (b) recognized intact but not cleaved GP, were assessed for cooperative binding to Jurkat cell surface displayed EBOV GP in the presence of the GP base-specific mAbs EBOV-515 or EBOV-520 (described below). This screening approach resulted in identification of broadly-reactive glycan cap region-specific mAbs EBOV-437, EBOV-442, and EBOV-548. Antibodies EBOV-442 and EBOV-548 potently neutralized EBOV and BDBV and offered partial protection (80 to 40% survival) *in vivo* in mice lethally challenged with live EBOV. mAb EBOV-548 showed the highest cooperativity with EBOV-515 and EBOV-520; based on this feature it was selected for further testing in the cocktail with EBOV-520.

mAb isotype and gene sequence analysis

The isotype and subclass of secreted antibodies were determined using murine anti-human IgG1, IgG2, IgG3 or IgG4 mouse antibodies conjugated with alkaline phosphatase (Southern Biotech). Antibody heavy- and light-chain variable region genes were sequenced from RNA obtained from hybridoma lines that had been cloned biologically by flow cytometric sorting. Total RNA was extracted using the RNeasy Mini kit (QIAGEN). A modified 5′RACE (Rapid Amplification of cDNA Ends) approach was used (Turchaninova et al., 2016). Briefly, 5 μL total RNA was mixed with cDNA synthesis primer mix (10 μM each) and incubated for 2 min at 70°C and then decrease the incubation temperature to 42°C to anneal the synthesis primers (1-3 min). After incubation, a mixture

containing 5X first-strand buffer (Clontech), DTT (20 mM), 5′ template switch oligo (10 μM), dNTP solution (10 mM each) and 10X SMARTScribe Reverse Transcriptase (Clontech) was added to the primer-annealed total RNA reaction and incubated for 60 min at 42°C. The first-strand synthesis reaction was purified using the Ampure Size Select Magnetic Bead Kit at a ratio of 1.8X (Beckman Coulter). Following, a single PCR amplification reaction containing 5 μL first-strand cDNA, 2X Q5 High Fidelity Mastermix (NEB), dNTP (10 mM each), forward universal primer (10 μM) and reverse primer mix (0.2 μM each in heavy-chain mix, 0.2 μM each in light-chain mix) were subjected to thermal cycling with the following conditions: initial denaturation for 1 min 30 s followed by 30 cycles of denaturation at 98°C for 10 s, annealing at 60°C for 20 s, and extension at 72°C for 40 s, followed by a final extension step at 72°C for 4 min. All primer sequences used in this protocol were previously described (Turchaninova et al., 2016). The first PCR reaction was purified using the Ampure Size Select Magnetic Bead Kit at a ratio of 0.6X (Beckman Coulter). Amplicon libraries were then prepared according to the Pacific Biosciences Multiplex SMRT Sequencing protocol and sequenced on a Pacific Biosciences Sequel platform. Raw sequencing data was demultiplexed and circular consensus sequences (CCS) were determined using the Pacific Biosciences SMRT Analysis tool suite. The identities of gene segments, CDRs, and mutations from germlines were determined by alignment using the ImMunoGeneTics database (Giudicelli and Lefranc, 2011).

mAb production and purification

For recombinant mAb production, cDNA encoding the genes of heavy and light chains were cloned into DNA plasmid expression vectors encoding IgG1 or IgG1-LALA - or Fab- heavy chain (McLean et al., 2000) and transformed into *E. coli* cells. mAb proteins were produced after transient transfection of ExpiCHO cells following the manufacturer's protocol and were purified from filtered culture supernatants by fast protein liquid chromatography (FPLC) on an ДKTA instrument using HiTrap MabSelect Sure column (GE Healthcare Life Sciences). Purified mAbs were buffer exchanged into PBS, filtered using sterile 0.45-μm pore size filter devices (Millipore), concentrated, and stored in aliquots at −80°C until use.

GP expression and purification

The ectodomains of EBOV GP ΔTM (residues 1-636; strain Makona; GenBank: KM233070), BDBV GP ΔTM (residues 1-643; strain 200706291 Uganda; GenBank: NC_014373), SUDV GP ΔTM (residues 1-637; strain Gulu; GenBank: NC_006432), and MARV GP ΔTM (residues 1-648; strain Angola2005; GenBank: DQ447653) were expressed and purified as described before (Gilchuk et al., 2018).

ELISA binding assays

Wells of microtiter plates were coated with purified, recombinant EBOV, BDBV, SUDV, or MARV GP ΔTM and incubated at 4°C overnight. Plates were blocked with 2% non-fat dry milk and 2% normal goat serum in DPBS containing 0.05% Tween-20 (DPBS-T) for 1 h. For mAb screening assays, hybridoma culture supernatants were diluted in blocking buffer 1:5, added to the wells, and incubated for 1 h at ambient temperature. The bound antibodies were detected using goat anti-human IgG conjugated with HRP (horseradish peroxidase) (Southern Biotech) and TMB (3,3′,5,5′-tetramethylbenzidine) substrate (ThermoFisher Scientific). Color development was monitored, 1N hydrochloric acid was added to stop the reaction, and the absorbance was measured at 450 nm using a spectrophotometer (Biotek). For dose-response and cross-reactivity assays, serial dilutions of purified mAbs were applied to the wells in triplicate or quadruplicate, and mAb binding was detected as detailed above.

Kinetics of mAb binding analysis by biolayer interferometry (BLI)

The Octet Red^{TM} 96e instrument (FortйBio, Pall) was used to assess binding kinetics of indicated mAbs to EBOV GP. Streptavidin sensors (Forte′Bio) were used to capture biotinylated EBOV GP 0.5 mg/mL in 1X kinetics buffer (PBS containing 0.002% Tween-20 and 0.1 or 2% bovine serum albumin (BSA; Sigma-Aldrich), as indicated. Binding was performed using serial two-fold dilutions of mAbs. The baseline and dissociation steps were carried out in the 1X kinetics buffer at 30 or 37°C as per the vendor's recommendations. Kinetic binding data are adequately described by 1:1 binding model but accounting for trimeric nature of immobilized GP and bivalent IgG analyte the associating stoichiometry is likely reflected more complex avidity effects. Therefore, data represent an apparent K_D values (K_D^{app}; Table S1), as previously described (Davidson et al., 2015).

Cell surface displayed GP mAb binding

Binding to Jurkat cell surface displayed EBOV, BDBV, or SUDV GPs was assessed with mAbs that were directly fluorescently-labeled. Briefly, mAbs were labeled with AF647 NHS ester (ThermoFisher Scientific) by following the manufacturer's protocol. Labeled mAbs were buffer exchanged into PBS using desalting Zeba columns (ThermoFisher Scientific) and stored at 4°C with 0.1% BSA (Sigma-Aldrich) and 0.01% sodium azide. Cells were washed with the incubation buffer containing DPBS (Dulbecco's phosphate-buffered saline), 2% of heat-inactivated FBS and 2 mM EDTA (ethylenediaminetetraacetic acid, sodium salt) (pH 8.0) by centrifugation at 400 x *g* for 5 min at ambient temperature.

For antibody staining, ~5 ц 10^4 cells were added per each well of V-bottom 96-well plate (Corning) in 5 μL of the incubation buffer. Serial dilutions of antibody were added to the cells in triplicate or quadruplicate for total volume of 50 μL per well, followed by 1 h incubation at room temperature, or 4°C in some experiments. Unbound antibody was removed by washing with 200 μL of the incubation buffer. Staining of cells was measured by flow cytometric analysis using an IntelliCyt iQue Screener Plus high throughput cytometer (Intellicyt Corp.). Data for up to 20,000 events were acquired, and data were analyzed with ForeCyt (Intellicyt Corp.)

software. Dead cells were excluded from the analysis on the basis of forward and side scatter gate for viable cell population. Binding to un-transduced Jurkat cells or binding of dengue antigen-specific mAb DENV 2D22 served as negative controls for most experiments. In some experiments, cells were fixed with 4% paraformaldehyde (PFA) in DPBS after staining and before flow cytometric analysis.

To assess binding of mAbs to cleaved GP, Jurkat-EBOV, -BDBV, or -SUDV GP cells were treated with 0.5 mg/mL of thermolysin (Promega) in PBS for 20 min at 37°C. Cells staining and flow cytometric analysis was performed as described above. The reaction was inhibited by washing cells with the incubation buffer containing DPBS, 2% of heat-inactivated FBS and 2 mM EDTA (pH 8.0). Binding to un-transduced Jurkat (mock) or uncleaved Jurkat-EBOV GP served as controls. EC_{50} values for saturated binding of mAb to GP_{CL} were determined using Prism 7.2 software (GraphPad) after log transformation of mAb concentration and median fluorescence intensity (MFI) values using sigmoidal dose-response nonlinear regression analysis. For non-saturating mAb binding, which observed with intact GP, EC_{50} values were calculated by linear regression analysis using EC_{50} and maximum response (Bmax) values that determined from saturating binding to GP_{CL} as above.

Cooperative binding to cell surface displayed GP

The assay was performed as described previously (Gilchuk et al., 2018). Briefly, Jurkat-EBOV, BDBV, or SUDV GP cells were incubated in triplicates with AF647-labeled first mAb alone (typically the GP-base specific mAb) or the same labeled mAb that titrated into a fixed concentration (typically 10 to 20 μg/mL) of the unlabeled second mAb (typically the GP glycan cap specific mAb). Cells were washed, and antibody binding was analyzed by flow cytometry using IntelliCyt iQue Screener Plus flow cytometer. Background values were determined from binding of the fluorescently labeled mAb to un-transduced (mock) Jurkat cells. Maximal values for saturated binding of rEBOV-520 or rEBOV-548 were estimated from the dose-response binding curves of the GP-base specific mAb rEBOV-520 with respective cell surface displayed cleaved GPs (GP_{CL}), which was based on a similar ratio of AF647 conjugation to rEBOV-520 and rEBOV-548. Results are expressed as the percent of maximal binding minus background signal from mock control for each tested condition with labeled mAb.

Epitope mapping using an EBOV GP alanine-scan mutation library

Epitope mapping was carried out as described previously (Davidson et al., 2015). Comprehensive high-throughput alanine scanning ('shotgun mutagenesis') was carried out on an expression construct for EBOV GP lacking the mucin-like domain (residues 311-461) (based on the Yambuku-Mayinga variant GP sequence), mutagenizing GP residues 33-310 and 462-676 to create a library of clones, each representing an individual point mutant. Residues were changed to alanine (with alanine residues changed to serine). The resulting library, covering 492 of 493 (99.9%) of target residues, was arrayed into 384-well plates, one mutant per well, then transfected into HEK293T cells and allowed to express for 22 h. Cells, unfixed or fixed in 4% PFA, were incubated with primary antibody and then with an AF488-conjugated secondary antibody (Jackson ImmunoResearch Laboratories). After washing, cellular fluorescence was detected using the Intellicyt flow cytometer. mAb reactivity against each mutant EBOV GP clone was calculated relative to wild-type EBOV GP reactivity by subtracting the signal from mock-transfected controls and normalizing to the signal from wild-type GP-transfected controls. Mutated residues within clones were identified as critical to the mAb epitope if they did not support reactivity of the test mAb but did support reactivity of other control EBOV mAbs. This counter-screen strategy facilitated the exclusion of GP mutants that were misfolded locally or that exhibited an expression defect (Davidson and Doranz, 2014).

Generation of virus neutralization escape mutants

To generate escape mutants, 100 PFU of EBOV-eGFP were combined with 2-fold dilutions of the respective mAb starting at 200 μg/mL in U-bottom 96-well plates and incubated for 1 h at 37°C. Mixtures were applied on Vero-E6 cell monolayer cultures in 96-well plates and incubated for 1 h. Supernatants were removed, freshly-diluted mAb was added at the same concentrations in 200 μL of MEM supplemented with 2% FBS, and plates were incubated for 7 days at 37°C. Viruses that replicated in the presence of the highest concentrations of mAb, as determined by monitoring eGFP fluorescence by microscopy, were collected. Twenty (20) μL aliquots were incubated with 2-fold dilutions of mAbs starting at 200 μg/mL, and viruses were propagated in the presence of mAbs as described above. The procedure was repeated once more with mAb dilutions starting at 400 μg/mL. Viruses that replicated at the highest mAb concentrations were amplified in Vero-E6 cell culture monolayers in 24-well plates in the presence of mAbs at 200 μg/mL for 7 days. Cellular RNA was extracted using TRIzol reagent, and cDNA copies of viral RNA encoding GP were amplified by RT-PCR and sequenced. To verify isolated escape mutants, 100 PFU of the viruses in MEM supplemented with 2% FBS in triplicate were combined in U-bottom 96-well plates with 8 to 12 two-fold dilutions of mAb, starting at 200 μg/mL and incubated for 1 h at 37°C. The virus/antibody mixtures then were applied in triplicate to Vero-E6 cell culture monolayers in 96-well plates, incubated for 1 h at 37°C, washed with MEM, overlaid with 200 μL of MEM containing 2% FBS and 0.8% methylcellulose, and incubated for 48 h at 37°C. Plates were fixed with 10% phosphate-buffered formalin (Fisher). Plaques were counted using fluorescence microscopy.

Neutralization assays

Virus neutralization assays were performed in a high-throughput format using the recombinant EBOV-eGFP or chimeric EBOV viruses in which GP was replaced with its counterpart from BDBV or SUDV, as described previously (Ilinykh et al., 2016). Briefly, four-fold dilutions of the respective mAb starting at 200 μg/mL were mixed in triplicate with 400 PFU of the virus in U-bottom

96-well plates and incubated for 1 h at 37°C. Mixtures were applied on Vero-E6 cell monolayer cultures in 96-well plates and incubated for four days at 37°C. In the absence of mAb neutralizing activity, the infection resulted in uniform eGFP fluorescence from the monolayer of cells that was readily detected by fluorescence microscopy. Fluorescence was measured using Synergy HT microplate reader (BioTek).

For assessing cooperative neutralization of SUDV by the cocktail of two mAbs, virus was incubated with increasing concentrations of rEBOV-520 or rEBOV-548 alone, or rEBOV-520 titrated into a fixed concentration (20 μg/mL) of rEBOV-548 in triplicate.

Real-time cell analysis assay (RTCA)

To screen for escape mutations in the presence of individual mAbs or the cocktail, we used a high-throughput and quantitative real-time cell analysis assay and xCELLigence Analyzer (ACEA Biosciences Inc.) that assesses kinetic changes in cell physiology, including virus-induced cytopathic effect (CPE). Fifty (50) μL of cell culture medium (DMEM supplemented with 2% FBS) was added to each well of a 96-well E-plate to obtain background reading. Eighteen thousand (18,000) Vero-E6 cells in 50 μL of cell culture medium were seeded per each well and plate was placed on the analyzer. Measurements were taken automatically every 15 min and the sensograms were visualized using RTCA software version 2.1.0 (ACEA Biosciences Inc). For the first passage, rVSV/EBOV GP or rVSV/SUDV GP viruses (0.3 MOI, ~6,000 PFU per well) were mixed with eight two-fold dilutions of individual mAbs or the cocktail of rEBOV-520/rEBOV-548 (1:1 mAbs ratio) starting at 25 μg/mL in a total volume of 100 μL and incubated for 1 h at 37°C. At 12 h after seeding the cells, the virus/mAb mixtures were added in 2 to 7 replicates to the cells in 96-well E-plates. Wells containing virus only in the absence of mAb and wells containing only Vero cells in medium were included on each plate as controls. Plates were measured continuously (every 15 min) for over 48 h to assess virus neutralization. Ten (10) μL aliquots from the wells with viruses that replicated at the highest mAb concentrations (~500-6,000 PFU) were used for the repeated passage for total 15 passages with rVSV/EBOV GP and 5 passages with rVSV/SUDV GP. The escape mutants were identified by CPE in wells containing typically neutralizing concentrations of mAbs. To verify the escape mutation, isolated viruses were tested with 100 μg/mL of each individual mAb and the cocktail using RTCA neutralization assay, and then sequenced. Controls included viruses from the late passages that did not escape neutralization in the presence of the cocktail, and viruses incubated in a presence of control mAb DENV 2D22. These viruses were assessed against individual mAbs (rEBOV-520, rEBOV-548, and DENV 2D22) and the cocktail, and then sequenced.

Rapid fluorometric antibody-mediated cytotoxicity assay (RFADCC)

Antibody-dependent cell-mediated cytotoxicity (ADCC) activity of EBOV GP-reactive IgG or Fab was quantified with an EBOV-adapted modification of the RFADCC assay (Domi et al., 2018; Orlandi et al., 2016). Briefly, a target cell line was made by transfecting 293F cells with a full-length DNA expressing GP from the EBOV-Kikwit isolate followed by transfecting with two separate DNA constructs expressing eGFP and the chimeric CCR5-SNAP tag protein. The new cell line, designated EBOV GPkik-293FS eGFP CCR5-SNAP, expresses EBOV-Kikwit GP on the plasma membrane, eGFP in the cytoplasm and the SNAP-tag CCR5, which can be specifically labeled with SNAP-Surface AF647 (NEB), on the cell surface (Domi et al., 2018). A recombinant form of a human anti-EBOV GP mAb KZ52 (a neutralizing antibody) (IBT Bioservices) was used as a positive control and the unrelated human mAb DENV 2D22 as a negative control. The ADCC activity was quantified by incubating three-fold serial dilutions of mAbs with EBOV GPkik-293FS eGFP CCR5-SNAP target cells for 15 min at ambient temperature and then adding human PBMC as effector cells for 2 h at 37°C, after which cells were washed once with PBS, fixed with 2% PFA, stained and analyzed with an LSRII Fortessa flow cytometer (BD Biosciences). Data analysis was performed with FlowJo software (Tree Star Inc.). The percentage cytotoxicity of the mAb was determined as the number of target cells losing eGFP signal (by virtue of ADCC) but retaining the surface expression of CCR5-SNAP.

Antibody-mediated cellular phagocytosis by human monocytes (ADCP)

Recombinant EBOV GP ΔTM (IBT Bioservices) was biotinylated and coupled to AF488 Neutravidin beads (Life Technologies). Antibodies were diluted to 5 μg/mL in cell culture medium and incubated with beads for 2 h at 37°C. THP-1 monocytes (ATCC) were added at 2.5 ɥ 10^4 cells per well and incubated for 18 h at 37°C. Cells were fixed with 4% PFA and analyzed on a BD LSRII flow cytometer, and a phagocytic score was determined using the percentage of $AF488^+$ cells and the MFI of the $AF488^+$ cells. The glycan cap-specific mAb c13C6 (IBT Bioservices) was used as a positive control, and the DENV-specific mAb 2D22 was used as a negative control.

Antibody-mediated neutrophil phagocytosis (ADNP)

Recombinant EBOV GP ΔTM (IBT Bioservices) was biotinylated and coupled to AF488 Neutravidin beads (Life Technologies). Antibodies were diluted to 5 μg/mL in cell culture medium and incubated with beads for 2 h at 37°C. White blood cells were isolated from donor peripheral blood by lysis of red blood cells, followed by three washes with PBS. Cells were added at a concentration of 5.0 ɥ 10^4 cells/well and incubated for 1 h at 37°C. Cells were stained with CD66b (Pacific Blue, Clone G10F5; BioLegend), CD3 (AF00, Clone UCHT1; BD Biosciences), and CD14 (APC-Cy7, Clone MφP9; BD Biosciences), and fixed with 4% PFA, and analyzed by flow cytometry on a BD LSR II flow cytometer. Neutrophils were defined as $SSC\text{-}A^{high}$ $CD66b^+$, $CD3^-$, $CD14^-$. A phagocytic score was determined using the percentage of $AF488^+$ cells and the MFI of the $AF488^+$ cells. The glycan cap-specific mAb c13C6 (IBT Bioservices) was used as a positive control, and the DENV-specific mAb 2D22 was used as a negative control.

Antibody-dependent NK cell activation

Recombinant EBOV GP ΔTM (IBT Bioservices) was coated onto a MaxiSorp 96 well plates (Nunc) at 300 ng/well at 4°C for 18 h. Wells were washed three times with PBS and blocked with 5% BSA in PBS. Antibodies were diluted to 10 μg/mL in PBS, and added to the plates, and were incubated for an additional 2 h at 37°C. Unbound antibodies were removed by washing three times with PBS, and human NK cells freshly isolated from peripheral blood of human donors by negative selection (Stem Cell Technologies, Canada) were added at 5 ų 10^4 cells/well in the presence of 4 μg/mL brefeldin A (Sigma-Aldrich Aldrich) and 5 μg/mL GolgiStop (Life Technologies) and anti-CD107a antibody (PE-Cy5, Clone H4A3, BD Biosciences). Plates were incubated for 5 h at 37°C. Cells were stained for NK cell markers (CD56 PE-Cy7, clone B159, BD Biosciences; CD16 APC-Cy7, clone 3G8, BD Biosciences; CD3 AF700, clone UCHT1, BD Biosciences), followed by fixation and permeabilization with Fix and Perm (Life Technologies) according to the manufacturer's instructions to stain for intracellular IFNγ (APC, Clone B27, BD Biosciences) and MIP-1β (PE, Clone D21-1351, BD Biosciences). Cells were analyzed on a BD LSRII flow cytometer. The glycan cap-specific mAb c13C6 (IBT Bioservices) was used as a positive control, and the DENV-specific mAb 2D22 was used as a negative control.

Mouse challenge

For EBOV challenge study, groups of 7-8-week-old female BALB/c mice (n = 5 per group) were inoculated with 1,000 PFU of the EBOV-MA by the intraperitoneal (i.p.) route. Mice were treated i.p. with 100 μg (∼5 mg/kg) of individual mAb per mouse on 1 dpi. Human mAb DENV 2D22 served as negative control. Mice were monitored twice daily from day 0 to 14 dpi for illness, survival, and weight loss, followed by once daily monitoring from 15 dpi to the end of the study at 28 dpi. The extent of disease was scored using the following parameters: score 1 – healthy; score 2 –ruffled fur and hunched posture; score 3 – a score of 2 plus one additional clinical sign such as orbital tightening and/or > 15% weight loss; score 4 – a score of 3 plus one additional clinical sign such as reluctance to move when stimulated, or any neurologic signs (seizures, tremors, head tilt, paralysis, etc.), or > 20% weight loss. Animals reaching a score of 4 were euthanized as per the IACUC-approved protocol. All mice were euthanized on day 28 after EBOV challenge. For SUDV challenge study, groups of 7-8-week-old *Stat1*$^{-/-}$ mice (n = 5 per group) were inoculated i.p. with 1,000 PFU wt SUDV (Gulu). Animals were treated i.p. with indicated doses of indicated individual mAbs or two-antibody cocktail on 1 dpi and were monitored as above.

NHP challenge

Five healthy adult rhesus macaques (*Macaca mulatta*) of Chinese origin (4 to 6 kg body weight) were studied. All animals were inoculated by i.m. route with a target dose of ∼1,000 PFU of EBOV isolate 199510621 (variant Kikwit) originated from a 65-year-old female patient who had died on 5 May 1995. The study challenge material was from the second Vero E6 passage of EBOV isolate 199510621. Briefy, the first passage at UTMB consisted of inoculating CDC 807223 (passage 1 of EBOV isolate 199510621) at a MOI of 0.001 onto Vero E6 cells. The cell culture fluids were subsequently harvested at day 10 post infection and stored at −80°C as ∼1 mL aliquots. Deep sequencing indicated the EBOV was greater than 98% 7U (consecutive stretch of 7 uridines). No detectable mycoplasma or endotoxin were measured (< 0.5 endotoxin units (EU)/mL). The back titer of the inoculum identified 1,025 PFU as the actual inoculation dose. Animals were randomized by random number assignment (with Microsoft Excel) into a treatment group of six animals and a control animal. The five EBOV-inoculated macaques in the treatment group received 30 mg/kg rEBOV-520 LALA + rEBOV-548 IgG1 (1:1) mAb mixture on days 3 and 6 after virus challenge by intravenous injection. Antibody concentration was ∼20 mg/mL resulting in an administered volume of 1.5 mL/kg. The control animal was not treated. Historical untreated controls included nine animals from three separate studies that were challenged with the same target dose of EBOV and by the same route. All animals were given physical exams, and blood was collected at the time of inoculation and at indicated times after EBOV inoculation. In addition, all animals were monitored daily and scored for disease progression with an internal filovirus scoring protocol approved by the UTMB Institutional Animal Care and Use Committee. The scoring measured from baseline and included posture or activity level, attitude or behavior, food and water intake, respiration, and disease manifestations such as visible rash, hemorrhage, ecchymosis, or flushed skin. A score of ≥ 9 indicated that an animal met criteria for euthanasia. These studies were not blinded.

Detection of virus load by plaque assay or quantitative reverse transcription PCR analysis (qRT-PCR)

Titration of virus in plasma samples and 10% tissue homogenates (w/v) was performed by plaque assay in Vero E6 cell culture monolayers. Briefly, increasing 10-fold dilutions of the samples were applied to Vero E6 cell monolayers in duplicate wells (200 μL); the limit of detection was 25 PFU/mL for plasma and 250 PFU/gram for tissue. For qRT-PCR analysis, RNA was isolated from whole blood or tissue using the Viral RNA Mini-kit (QIAGEN) using 100 μL of blood or 100 mg of tissue into 600 μL of buffer AVL. Primers (probe) targeting the VP35 intergenic region of EBOV were used for qRT-PCR with the probe sequence of 6-carboxyfluorescein (6FAM)-5′ CCGTCAATCAAGGAGCGCCTC 3′-6 carboxytetramethylrhodamine (TAMRA) (ThermoFisher Scientific). EBOV RNA was detected using the CFX96 detection system (BioRad Laboratories) in One-step probe qRT-PCR kits (QIAGEN) with the following cycle conditions: 50°C for 10 min, 95°C for 10 s, and 40 cycles of 95°C for 10 s and 57°C for 30 s. Threshold cycle (CT) values representing EBOV genomes were analyzed with CFX Manager Software, and data are depicted as genome equivalents (GEq); the limit of detection was 3.7 $\log_{10}$GEq/mL for blood and 3.7 $\log_{10}$GEq/g for the tissues.

NHP serum biochemistry

Serum samples collected from NHPs were tested for concentrations of albumin, amylase, alanine aminotransferase, aspartate aminotransferase, alkaline phosphatase, gamma-glutamyltransferase, glucose, cholesterol, total protein, blood urea nitrogen, creatinine, uric acid, and C-reactive protein by using a Piccolo point-of-care analyzer and Biochemistry Panel Plus analyzer discs (Abaxis).

Detection of circulating human mAbs in NHP serum

ELISA plates were coated overnight at 4°C with 0.1 μg/mL of mouse anti-human IgG (human CH2 domain with no cross-reactivity to rhesus macaque IgG; clone R10Z8E9; BioRad) and then blocked for 2 h. The serum samples were assayed at 4-fold dilutions starting at a 1:100 dilution in ELISA diluent (PBS containing 1% heat-inactivated FBS and 0.2% Tween-20). Samples were incubated for 1 h at ambient temperature and then removed, and plates were washed. Wells then were incubated for 1 h with goat anti-human IgG conjugated to HRP (ThermoFisher Scientific) at a 1:20,000 dilution. Wells were washed and then incubated with TMB substrate (KPL) (100cμL/well) and incubated for 10cmin followed by 1N hydrochloric acid stop the reaction (100cμL/well). Microplates are read at 450cnm with 650cnm subtraction with an OD_{450}cnm cut-off of 0.052 (Biotek Cytation reader). Human mAbs were quantified using Prism software, version 7.04 (GraphPad), to analyze sigmoidal dose-response (variable slope), using 1:1 mixture of rEBOV-520 LALA and rEBOV-548 IgG1 cocktail as a standard.

Single particle negative stain electron microscopy

Antibody Fabs were obtained by digesting IgG with 4% papain (w/w) and affinity purified using a CaptureSelectIgG-CH1 affinity column (ThermoFisher Scientific). Fab was further purified by size exclusion chromatography (SEC) using an S200I column (GE Healthcare Life Sciences) equilibrated in 1X TBS (20 mM Tris, 150 mM NaCl, pH 7.4). rEBOV-520 and/or rEBOV-548 Fab were added to EBOV GP ΔTM trimer in molar excess and incubated for 4 h on ice. Complexes were then added directly to copper 400 mesh grids (Electron Microscopy Sciences) that had been thinly coated with carbon and stained with a solution of 2% (w/v) uranyl formate. Negative stain images were collected on a 120 KeV Tecnai Spirit equipped with a 4kx4k TemCam 4F16 CMOS camera. Micrographs were collected using Leginon (Potter et al., 1999) and processed on Appion (Lander et al., 2009). Particles were picked using DoG picker (Voss et al., 2009), extracted and aligned using MSA/MRA (Zhao and Singer, 2014) reference-free 2D classification. Particles were further classified using Relion (Scheres, 2012) by 3D classification, and homogeneous classes were further refined.

Single particle cryogenic electron microscopy

EBOV GP ΔMucΔTM (Makona strain) was produced in 293F cells and purified as described previously (Murin et al., 2018). rEBOV-520 Fab and rEBOV-548 Fab were produced recombinantly as described above. rEBOV-548 was added to 300 μg GP in 5M excess the first and allowed to incubate overnight at 4°C. The complex was purified by SEC on an S200I column using 1X TBS. A 5M excess of rEBOV-520 Fab and ADI-16061 Fab were then added to the purified GP−rEBOV-548 complex and allowed to incubate at 4°C for 4 h. A recombinant form of ADI-16061 Fab used for cryo-EM was generated as previously described (Murin et al., 2018). The complex containing rEBOV-520, rEBOV-548 and ADI-16061 was then concentrated to 5 mg/mL using a 100 kDa MWCO spin column (Millipore) that had been equilibrated in 1X TBS. The complex was diluted to 4 mg/mL using 1X TBS and mixed with 0.01% (w/v) Fluorinated Octyl Maltoside (Anatrace), after which 3 μL was applied to 1.2/1.3-4C 400 mesh Cu grids (Quantifoil) that had been plasma cleaned with a mixture of Ag/O_2 for 10 s (Gatan Solarus 950 Plasma System). Samples were vitrified using a Vitrobot (Thermo Fisher) equilibrated at 4°C in an environment of 100% humidity. Grids with sample applied were equilibrated for 10 s, followed by 0-force blotting on both sides of the grid using Whatman No. 1 filter paper for a total of 4.5 s. The complex of EBOV GP ΔMucΔTM (Makona strain) bound to rEBOV-548 and ADI-16061 Fabs was prepared in the same manner as described above.

Cryo-EM data were collected as listed in Table S4. Raw micrographs were aligned and dose-weighted using MotionCorr2 (Zheng et al., 2017) followed by whole micrograph CTF-collection using GCTF (Zhang, 2016). Template-based picking, particle extraction and reference-free 2D classification were all performed using Cryosparc2 (Punjani et al., 2017). For the EBOV GP ΔMucΔTM−rEBOV-548−rEBOV-520 complex, cleaned particle stacks were then re-extracted in RELION 3.0 (Zivanov et al., 2018), followed by 3D-classification using C1 symmetry. A tight mask was generated around the GP core and rEBOV-548 Fabs and an additional round of classification was performed with tighter angular sampling. This procedure revealed several substates of the complex, with portions of the glycan cap in different positions in each protomer position. A single class with 13,144 particles was selected based off of estimated resolution and due to the appearance of C3 symmetry, indicating that all three of the glycan cap protomers were in the same position in this class. Particles from this class were re-extracted and 3D-refinement was performed using a tight mask that just contained the Fv domains of rEBOV-520 and rEBOV-548 as well as the GP core and C3 symmetry was applied. Local resolution estimation and angular sampling was also performed using RELION 3.0. For the EBOV GP ΔMucΔTM−rEBOV-548 complex, all processing was performed exclusively in Cryosparc2. An *ab initio* initial model was generated first and then used to back-project a cleaned stack using C3 symmetry and non-uniform refinement with an experimentally generated mask around the entire GP core and rEBOV-548 Fabs.

For modeling, a cryo structure of EBOV GP ΔMucΔTM (Makona) (PDB: 6DZL) was used as an initial model. For Fabs, initial models were generated using Swiss Modeler (Biasini et al., 2014). These components were fit into the EM density using UCSF Chimera (Pettersen et al., 2004) and a single round of real-space refinement was performed in Phenix (Adams et al., 2010) using NCS and secondary structure constraints. The resulting model was then refined in Rosetta (DiMaio et al., 2015). For each round of refinement, 319 models were produced and evaluated using MolProbity (Williams et al., 2018) and EMRinger (Barad et al., 2015). Idealized

glycans were then added and trimmed to fit EM density using the model with the best statistics, followed by manual adjustment in Coot (Emsley et al., 2010) followed by a final round of refinement in Rosetta, including glycans and restraining backbone coordinates. For the EBOV GP ΔMucΔTM (Makona) complex with rEBOV-548 alone, an additional refinement in Phenix was performed to idealize geometry. Glycans were validated using PDB-care (Lütteke and von der Lieth, 2004) and Privateer (Agirre et al., 2015). All model figures were generated using UCSF Chimera (Pettersen et al., 2004). To estimate change in GP solvent exclusion upon Fabs binding, GP1,2 from an unliganded GP structure (PDB: 5JQ3), and GP1,2 bound to the respective Fabs were used to create a surface map in UCSF chimera (Pettersen et al., 2004) and then normalized to Gly-X-Gly tripeptides (Bendell et al., 2014) to determine a normalized solvent excluded surface (SES).

Epitope mapping using peptide fragmentation and hydrogen-deuterium exchange mass spectrometry (HDX-MS)

To maximize peptide sequence coverage, the optimized digestion and quench conditions were determined prior to deuteration studies. Briefly, EBOV GP ΔTM or EBOV GP_{CL} samples were diluted with DPBS buffer (150 mM NaCl, 1.9 mM KH_2PO_4, pH = 7.4) at 0°C and then quenched with 0.8% formic acid (v/v) containing various concentration of guanidine hydrochloride (GuHCl; 0.8-8 M) and Tris(2-carboxyethyl) phosphine (TCEP) (0.1 or 1.0 M). Eight (8) M GuHCl, 0.5 M TCEP in PBS pH = 2.0 gave an optimal peptide coverage map.

Hydrogen-deuterium exchange reactions were initiated by diluting protein samples with D_2O in DPBS buffer at a 1:2 ratio (v/v) at 10 s, 100 s or 1,000 s prior to quenching and on-line pepsin digestion. Non-deuterated samples served as controls. Using a Waters nano-ACQUITY UPLC system with an HDX manager (Waters Corp.), samples were injected onto an immobilized pepsin column (Waters Enzymate^{TM}) where digestion was performed at 20°C and 4,700 psi at a flow of 100 μL/min of 0.1% formic acid in H_2O. The resulting peptides were collected on a VanGuard BEH C18 1.7 μm guard column (Waters Corp.) and separated over a Waters BEH C18 1.7 μm, 1 mm x 100 mm column using a gradient of 5%–25% acetonitrile over 6 min. The column was coupled to a Waters Xevo G2-XS instrument, eluent was electrosprayed, and MS^E scans were performed with lock-mass acquisition (Leucine enkephalin, m/z 556.2771). The capillary was set to 2.8kV, source temperature to 80°C, desolvation temperature to 175°C, desolvation gas to 400 L/h and the instrument was scanned over a m/z range of 50-2,000. All experiments were carried out in triplicate. Waters ProteinLynx LGobal Server 3.0.3 software (Waters Corp.) was used to identify the peptide ions with an FDR of 4%, using non-specific protease cleavage, a minimum number of fragment ion matches per peptide of three, and oxidation of methionine as variable modification. DynamX 3.0 (Waters Corp) was used for the analysis of the mass spectra. Non-deuterated samples and equilibrium-deuterated back-exchange control samples served as controls. The centroids of the isotopic envelopes of non-deuterated, functionally deuterated, and fully deuterated peptides were measured using DXMS Explorer, and then converted to corresponding deuteration levels with corrections for back-exchange.

Crystallography and structure determination

EBOV GP for co-crystallization with EBOV-520 was expressed as mucin-like domain-deleted GP (GP ΔMuc) in *Drosophila* S2 cells using a single pMT-puro plasmid encoding a C-terminally Strep-tagged construct lacking the transmembrane domain. The protein was purified using a StrepTrap HP affinity chromatography column (GE Healthcare Life Sciences) followed by cleavage of the Strep tag at an Enterokinase cleavage site using EKMax (ThermoFisher Scientific). To prepare GP_{CL}, purified GP ΔMuc was incubated with 1.5% thermolysin overnight at room temperature to mimic endosomal cathepsin cleavage followed by further purification using a Superdex 200 Increase 10/300 GL SEC column (GE Healthcare Life Sciences). EBOV-520 Fab for co-crystallization with EBOV GP_{CL} was prepared by incubating EBOV-520 IgG with 2% papain for 4 h at 37°C; the digestion was quenched using 50 mM iodoacetamide. The Fab was purified from the reaction mixture using a MonoQ 5/50 GL ion-exchange column (GE Healthcare Life Sciences) followed by further purification using a Superdex 75 Increase 10/300 GL SEC column (GE Healthcare Life Sciences).

The GP_{CL}-EBOV-520 Fab complex was obtained by incubating GP_{CL} with a 3-fold molar excess of EBOV-520 Fab overnight at 4°C followed by purification using a Superdex 200 Increase 10/300 GL SEC column (GE Healthcare Life Sciences). The complex was screened for crystallization using a Douglas Instruments Oryx8, and the protein crystallized in a solution of 0.1 M HEPES pH 7.0 and 1.4 M ammonium sulfate. Diffraction data to 3.46 Å resolution were collected at beamline 23-IDD at the Advanced Photon Source. The diffraction images were processed using iMosflm (Battye et al., 2011) and scaled using Aimless (Evans and Murshudov, 2013). Molecular replacement, model building, and structure refinement were carried out using the PHENIX suite of programs (Adams et al., 2010). Chains G and H of the PDB entry 5HJ3 were used as molecular replacement search models for GP_{CL}, and chains Y and Z of the PDB entry 4YK4 were used as a search model for EBOV-520 Fab following model pruning using Sculptor (Bunkyczi and Read, 2011). The molecular graphics application Coot (Emsley et al., 2010) was used for model inspection and manual refinement. A single GP_{CL} monomer and a single EBOV-520 Fab were contained within the asymmetric unit of the $P4_132$ crystals, and crystal symmetry was applied to generate the model of the biologically relevant trimer shown in all figures.

QUANTIFICATION AND STATISTICAL ANALYSIS

The descriptive statistics mean ± SEM or mean ± SD were determined for continuous variables as noted. Survival curves were estimated using the Kaplan Meier method and curves compared using the two-sided log rank test (Mantel-Cox) with subjects right censored, if they survived until the end of the study. EC_{50} values for mAb binding were determined after log transformation of antibody concentration using sigmoidal dose-response nonlinear regression analysis. In neutralization assays, IC_{50} values were

calculated after log transformation of antibody concentrations using a 3-parameter nonlinear fit analysis. The effect of antibody composition on the GP binding (single mAb or two-antibody mixture) and p values were estimated by overall test from untransformed MFI flow cytometric values using two-way ANOVA. In neutralization assays, mAb synergy by cocktails was quantified with CompuSyn software using approach that estimates the combination index (CI) to define the effect of drug combination (Chou, 2010). CI values were calculated for each tested concentration of mAb combination, and CI values < 1 considered as evidence of synergy. Viral titers in plasma were compared using a Wilcoxon signed-rank test (two-tailed) where column medians compared to a value that equals to the limit of detection for the plaque assay (1.4 $\log_{10}$ PFU/mL). $p < 0.05$ considered as significant. Technical and biological replicates are indicated in the figure legends. Statistical analyses were performed using Prism v7.2 (GraphPad).

DATA AND CODE AVAILABILITY

The EBOV GP_{CL}–EBOV-520 Fab crystal structure, the EBOV GP ΔMuc ΔTM (Makona)–rEBOV-520–rEBOV-548 Fab cryo-EM structure, and EBOV GP ΔMuc ΔTM (Makona)–rEBOV-548 Fab structure has been deposited in the PDB with accession code 6OZ9, 6PCI, and 6UYE respectively. The accession numbers for the negative stain and cryo-EM reconstructions reported in this paper have been deposited to the Electron Microscopy Data Bank under accession numbers EMDB: EMD-20293, EMD-20301, and EMD-20947 (see Key Resources Table for details), respectively. All relevant data are included with the manuscript; source data for each of the display items is provided in Key Resources Table.